PETIMOT: A NOVEL FRAMEWORK FOR INFERRING PROTEIN MOTIONS FROM SPARSE DATA USING SE(3)-EQUIVARIANT GRAPH NEURAL NETWORKS

Anonymous authors

Paper under double-blind review

ABSTRACT

Proteins move and deform to ensure their biological functions. Despite significant progress in protein structure prediction, approximating conformational ensembles at physiological conditions remains a fundamental open problem. This paper presents a novel perspective on the problem by directly targeting continuous compact representations of protein motions inferred from sparse experimental observations. We develop a task-specific loss function enforcing data symmetries, including scaling and permutation operations. Our method PETIMOT (Protein sEquence and sTructure-based Inference of MOTions) leverages transfer learning from pre-trained protein language models through an SE(3)-equivariant graph neural network. When trained and evaluated on the Protein Data Bank, PETIMOT shows superior performance in time and accuracy, capturing protein dynamics, particularly large/slow conformational changes, compared to state-of-the-art flow-matching approaches and traditional physics-based models.

1 Introduction

Proteins orchestrate biological processes in living organisms by interacting with their environment and adapting their three-dimensional (3D) structures to engage with cellular partners, including other proteins, nucleic acids, small-molecule ligands, and co-factors. In recent years, spectacular advances in high-throughput deep learning (DL) technologies have provided access to reliable predictions of protein 3D structures at the scale of entire proteomes (Varadi et al., 2024). These breakthroughs have also highlighted the complexities of protein conformational heterogeneity. State-of-the-art predictors struggle to model alternative conformations, fold switches, large-amplitude conformational changes, and solution ensembles (Chakravarty et al., 2025).

The success of AlphaFold2 (Jumper et al., 2021) has stimulated machine-learning approaches focused on inference-time interventions in the model to generate structural diversity. They include enabling or increasing dropout (Raouraoua et al., 2024; Wallner, 2023), or manipulating the evolutionary information given as input to the model (Kalakoti & Wallner, 2024; Wayment-Steele et al., 2023; Del Alamo et al., 2022; Stein & Mchaourab, 2022). Despite promising results on specific families, several studies have emphasised the difficulties in rationalising the effectiveness of these modifications and interpreting them (Porter et al., 2024; Bryant & Noé, 2024). Moreover, these cannot be transferred to protein language model-based predictors that do not rely on multiple sequence alignments. Researchers have also actively engaged in the development of deep learning frameworks based on diffusion, or the more general flow matching, to generate conformational ensembles (Lewis et al., 2025; Wang et al., 2025). While being several orders of magnitude cheaper than Molecular Dynamics (MD) simulations, these models remain computationally intensive, require massive MD training data, and are limited to sampling approximate equilibrium distributions.

This work presents a new glance at the protein conformational diversity problem. Instead of learning and sampling from multi-dimensional empirical distributions, we propose to learn eigenspaces (the structure) of the positional covariance matrices in collections of experimental 3D structures and generalize these over different homology levels. The use of experimental structure collections to infer protein dynamics through Principal Component Analysis (PCA) is well-established in the literature (Best et al., 2006; Schneider et al., 2025; Lombard et al., 2024a; Yang et al., 2009). The diversity

present within – even a modest number of – experimental 3D structures of the same protein or close homologs is a good proxy for the conformational heterogeneity of proteins in solution (Best et al., 2006) and can generally be (almost fully) explained by a small set of linear vectors, also referred to as modes (Lombard et al., 2024a; Yang et al., 2009). Moreover, interpolation trajectories performed in PCA space inferred from experimental structures can recapitulate intermediate functional states (Lombard et al., 2024a). Although linear spaces may not be well-suited for capturing highly complex non-linear motions, such as loop deformations, they offer multiple advantages. These include faster learning due to the reduced complexity of the model, improved explainability as the components directly correspond to interpretable data dimensions, faster inference, and the straightforward combination or integration of multiple data dimensions.

To summarize, our main contributions are:

- We provide a novel formulation of the protein conformational diversity problem.
- We present a novel benchmark representative of the Protein Data Bank structural diversity and compiled with a robust pipeline (Lombard et al., 2024a), along with data- and taskspecific metrics.
- We develop a SE(3)-equivariant Graph Neural Network architecture equipped with a novel symmetry-aware loss function for comparing linear subspaces, with invariance to permutation and scaling. Our model, PETIMOT, leverages embeddings from pre-trained protein language models (pLMs), building on prior proof-of-concept work demonstrating that they encode information about functional protein motions (Lombard et al., 2024b).
- PETIMOT is trained on sparse experimental data without any use of simulation data, in contrast with Timewarp for instance (Klein et al., 2024). Moreover, our model does not require physics-based guidance or feedback, unlike (Wang et al., 2025) for instance.
- Our results demonstrate the capability of PETIMOT to generalise across protein families (contrary to variational autoencoder-based approaches) and to compare favorably in running time and accuracy to the physics-based Normal Mode Analysis.

2 RELATED WORKS

Protein structure prediction and generating conformational ensembles. AlphaFold2 was the first end-to-end deep neural network to achieve near-experimental accuracy in predicting protein 3D structures, even for challenging cases with low sequence similarity to proteins with resolved structures (Jumper et al., 2021). Later works have shown that substituting the input alignment by embeddings from a protein language model can yield comparable performance (Lin et al., 2023; Hayes et al., 2024; Weissenow et al., 2022; Wu et al., 2022).

Beyond the single-structure frontier, several studies have underscored the limitations and potential of protein structure predictors (PSP) for generating alternative conformations (Saldaño et al., 2022; Lane, 2023; Bryant & Noé, 2024; Chakravarty et al., 2025). Approaches focused on re-purposing AlphaFold2 include dropout-based massive sampling (Raouraoua et al., 2024; Wallner, 2023), guiding the predictions with state-annotated templates (Faezov & Dunbrack Jr, 2023; Heo & Feig, 2022), and inputting shallow, masked, corrupted, subsampled or clustered alignments (Kalakoti & Wallner, 2024; Wayment-Steele et al., 2023; Del Alamo et al., 2022; Stein & Mchaourab, 2022). Despite promising results, these approaches remain computationally expensive and their generalisability, interpretability, and controllability remain unclear (Bryant & Noé, 2024; Chakravarty et al., 2025). More recent works have aimed at overcoming these limitations by directly optimising PSP learnt embeddings under low-dimensional ensemble constraints (Yu et al., 2025).

Another line of research has consisted in fine-tuning or re-training AlphaFold2 and other single-state PSP under diffusion or flow matching frameworks (Jing et al., 2024; Abramson et al., 2024; Krishna et al., 2024). More generally, diffusion- and flow matching-based models allow for efficiently generating diverse conformations conditioned on the presence of ligands or cellular partners (Jing et al., 2023; Ingraham et al., 2023; Wang et al., 2025; Liu et al., 2024; Zheng et al., 2024). Despite their strengths, these techniques are prone to hallucination.

Parallel related works have sought to directly learn generative models of equilibrium Boltzmann distributions using normalising flows (Lewis et al., 2025; Noé et al., 2019; Klein et al., 2024), or

machine-learning force fields based on equivariant graph neural network (GNN) representations (Wang et al., 2024a), to enhance or replace molecular dynamics (MD) simulations. The BioEmu model (Lewis et al., 2025) predicts large and biologically meaningful conformational changes observed in the Protein Data Bank (PDB) (Berman et al., 2000) and approximates long MD simulations.

Protein conformational heterogeneity manifold learning. Unsupervised, physics-based Normal Mode Analysis (NMA) has long been effective for inferring functional modes of deformation by leveraging the topology of a single protein 3D structure (Grudinin et al., 2020; Hoffmann & Grudinin, 2017; Hayward & Go, 1995). While appealing for its computational efficiency, the accuracy of NMA strongly depends on the initial topology (Laine & Grudinin, 2021), limiting its ability to model extensive secondary structure rearrangements. Recent efforts have sought to address these limitations by directly learning continuous, compact representations of protein motions from sparse experimental 3D structures. These approaches employ dimensionality reduction techniques, from classical manifold learning methods (Lombard et al., 2024a) to neural network architectures like variational auto-encoders (Ramaswamy et al., 2021). By projecting motions onto a learned low-dimensional manifold, these methods enable reconstruction of accurate, physico-chemically realistic conformations, both within the interpolation regime and near the convex hull of the training data (Lombard et al., 2024a). Additionally, they assist in identifying collective variables from molecular dynamics (MD) simulations, supporting importance-sampling strategies (Chen et al., 2023a; Belkacemi et al., 2021; Bonati et al., 2021; Wang et al., 2020; Ribeiro et al., 2018). Despite these advances, such approaches are currently constrained to family-specific models.

E(3)-equivariant graph neural networks. Graph Neural Networks (GNN) have been extensively used to represent protein 3D structures. They are robust to transformations of the Euclidean group, namely rotations, reflections, and translations, as well as to permutations. In their simplest formulation, each node represents an atom and any pair of atoms are connected by an edge if their distance is smaller than a cutoff or among the smallest k interatomic distances. Many works have proposed to enrich this graph representation with SE(3)-equivariant features informing the model about interatomic directions and orientations (Ingraham et al., 2019; Jing et al., 2020; Dauparas et al., 2022; Krapp et al., 2023; Wang et al., 2024b). To go beyond local 3D neighbourhoods while maintaining sub-quadratic complexity, Chroma adds in randomly sampled long-range connections (Ingraham et al., 2023).

3 Data representation and problem formulation

To generate training data, we exploit experimental protein single chain structures available in the PDB. We first clustered these chains based on their sequence similarity. Then, within each cluster, we aligned the protein sequences and used the resulting mapping for superimposing the 3D coordinates (Lombard et al., 2024a). It may happen that some residues in the multiple sequence alignment do not have resolved 3D coordinates in all conformations. To account for this uncertainty, we assigned a confidence score w_i to each residue i computed as the proportion of conformations including this residue. The 3D superimposition puts the conformations' centers of mass to zero and then aims at determining the optimal least-squares rotation minimizing the Root Mean Square Deviation (RMSD) between any conformation and a reference conformation, while accounting for the confidence scores (Kabsch, 1976; Kearsley, 1989),

$$E = \frac{1}{\sum_{i} w_{i}} \sum_{i} w_{i} (\vec{r}_{ij} - \vec{r}_{i0})^{2}, \tag{1}$$

where $\vec{r}_{ij} \in \mathbb{R}^3$ is the *i*th centred coordinate of the *j*th conformation and $\vec{r}_{i0} \in \mathbb{R}^3$ is the *i*th centred coordinate of the reference conformation. Next, we defined our ground-truth targets as eigenspaces of the coverage-weighted $C\alpha$ -atom positional covariance matrix,

$$C = \frac{1}{m-1} R^c W(R^c)^T = \frac{1}{m-1} (R - R^0) W(R - R^0)^T,$$
 (2)

where R is the $3N \times m$ positional matrix with N the number of residues and m is the number of conformations, R^0 contains the coordinates of the reference conformation, and W is the $3N \times 3N$ diagonal coverage matrix. The covariance matrix is a $3N \times 3N$ square matrix, symmetric and real. We decompose C as $C = YDY^T$, where Y is a $3N \times 3N$ matrix with each column defining a

coverage-weighted eigenvector or a principal component that we interpret as a *linear motion*. D is a diagonal matrix containing the eigenvalues. The latter highly depend on the sampling biases in the PDB and thus we do not aim at predicting them.

Problem formulation. For a protein of length N, let Y be $3N \times K$ orthogonal ground-truth deformations,

$$Y^TY = I_K. (3)$$

Our goal is to find coverage-weighted vectors $X \in \mathbb{R}^{3N \times L}$ whose components l approximate some components k of the ground truth Y:

$$W^{\frac{1}{2}}\tilde{\mathbf{x}}_{l} \approx \mathbf{y}_{k}.\tag{4}$$

Below, we provide three alternative formulations for this problem. PETIMOT's loss function serves two key purposes: it enables effective training of the network to predict subspaces representing multiple distinct modes of deformations -i.e., with low overlap between the subspace's individual linear vectors, while preventing convergence to a single dominant mode.

The least-square formulation. To evaluate a predicted motion direction against a ground-truth direction, we use a Least-Square (LS) error, which, together with Mean Absolute Error (MAE), is among the most accepted metrics for regression tasks. Here, we have specifically adapted it to the challenge of evaluating directional motion vectors rather than static coordinates, and scaled between 0 and 1 for better training, interpretability and usability.

For each protein of length N with a coverage W, we compute the weighted pairwise *least-square* difference \mathcal{L}_{kl} between ground-truth directions Y and predicted motion directions X for each pair of a k direction in the ground truth and an k direction in the prediction as,

$$\mathcal{L}_{kl} = \frac{1}{N} \sum_{i=1}^{N} \|\vec{y}_{ik} - w_i^{1/2} c_{kl} \vec{x}_{il}\|^2 = \frac{1}{N} \mathbf{y}_k^T \mathbf{y}_k - \frac{1}{N} \frac{(\mathbf{y}_k^T W^{\frac{1}{2}} \mathbf{x}_l)^2}{\mathbf{x}_l^T W \mathbf{x}_l},$$
 (5)

where we scaled the ground-truth tensors such that $Y^TY = NI_K$ and we used the fact that the optimal scaling coefficients c_{kl} between the k-th ground truth vector and the l-th prediction are given by

$$c_{kl} = \frac{\sum_{i=1}^{N} w_i^{\frac{1}{2}} \mathbf{y}_{ik}^T \mathbf{x}_{il}}{\sum_{i=1}^{N} w_i \mathbf{x}_{il}^T \mathbf{x}_{il}} = \frac{\mathbf{y}_k^T W^{\frac{1}{2}} \mathbf{x}_l}{\mathbf{x}_l^T W \mathbf{x}_l}.$$
 (6)

This invariance to global scaling is motivated by the fact that we aim at capturing the relative magnitudes and directions of the motion patterns rather than their sign or absolute amplitudes.

Linear assignment problem. We then formulate an *optimal linear assignment problem* to find the minimum-cost matching between the ground-truth and the predicted directions. Specifically, we aim to solve the following assignment problem for the least-square (LS) costs,

LS Loss =
$$\min_{\pi \in S_J} \sum_{k=1}^{\min(K,L)} \mathcal{L}_{k,\pi(k)}$$

subject to:
 $\pi: \{1, \dots, \min(K, L)\} \to \{1, \dots, L\}, \ \pi(k) \neq \pi(k') \text{ for } k \neq k',$

where K and L are the number of ground-truth and predicted directions respectively, and $\pi(k)$ represents the index of the predicted direction assigned to the k-th ground truth direction. This formulation ensures an optimal one-to-one matching, while accommodating cases where the number of predicted and ground-truth directions differs. We backpropagate the loss only through the optimally matched pairs, using scipy linear_sum_assignment. We have also tested a smooth version of the loss above with continuous gradients, but it did not improve the performance.

The subspace coverage formulation. We propose another formulation of the problem in terms of the subspace coverage metrics (Amadei et al., 1999; Leo-Macias et al., 2005; David & Jacobs, 2011). Specifically, we sum up *squared sinus* (SS) dissimilarities between ground-truth and predicted directions (formally computed as one minus squared cosine similarity),

SS Loss =
$$1 - \frac{1}{K} \sum_{k=1}^{K} \sum_{l=1}^{K} (\mathbf{y}_{k}^{T} W^{\frac{1}{2}} \mathbf{x}_{l}^{\perp})^{2}$$
, (8)

where the subspace $\{\mathbf{x}_l^\perp\}$ is obtained by orthogonalising the coverage-weighted predicted linear subspace $\{W^{\frac{1}{2}}\mathbf{x}_l\}$, where $\mathbf{x}_l^TW\mathbf{x}_l=1$, using the Gram–Schmidt process. This operation ensures that the loss ranges from zero for identical subspaces to one for mutually orthogonal subspaces and avoids artificially inflating the SS loss due to redundancy in the predicted motions. The order in which the predicted vectors are orthogonalised does not influence the loss, guaranteeing stable training. Appendix A proves this statement. The SS loss is conceptually similar to the comparison of angles between subspaces – see a few recent examples of such subspace comparison from other ML domains in (Zhu et al., 2021; Feng et al., 2023; Chen et al., 2023b; Hawke et al., 2024; Schlaginhaufen & Kamgarpour, 2024).

Independent Subspace (IS) Loss. We can substitute the orthogonalisation procedure by using an auxiliary loss component for maximising the rank of the predicted subspace. For this purpose, we chose the squared cosine similarity computed between pairs of predicted vectors. The final expression for the *independent subspace* (IS) loss is

IS Loss =
$$\frac{1}{K^2} \sum_{k=1}^{K} \sum_{l=1}^{K} (\mathbf{x}_k^T W \mathbf{x}_l)^2 - \frac{1}{K^2} \sum_{k=1}^{K} \sum_{l=1}^{K} (\mathbf{y}_k^T W^{\frac{1}{2}} \mathbf{x}_l)^2,$$
(9)

where the predictions $\{\mathbf{x}_l\}$ are normalised prior to the loss computation such that $\mathbf{x}_l^T W \mathbf{x}_l = 1$ and the scaling factor K^2 ensures that the loss ranges between 0 and 1. Appendix A analyses the stability of this formulation.

4 ARCHITECTURE

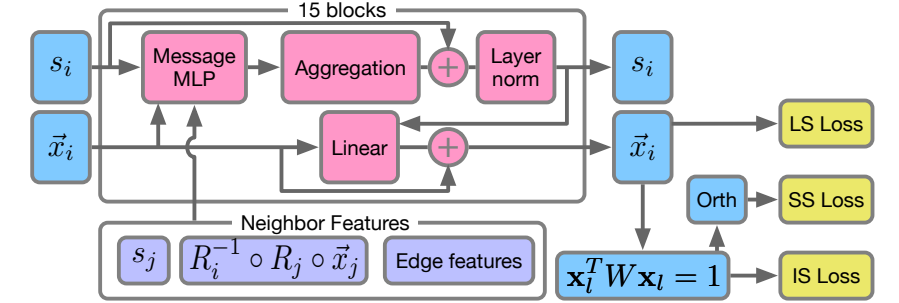


Figure 1: **PETIMOT's architecture overview.** The model processes both sequence embeddings (s) and motion vectors (\vec{x}) through 15 message-passing blocks. Each block updates both representations by aggregating information from neighboring residues. Neighbor features are computed in the reference frame of the central residue i, ensuring SE(3) equivariance. The geometric features encoded in the edges capture the relative spatial relationships between residue pairs. Three types of losses (LS, SS, and IS) are computed, with prior normalization of the predictions for the IS and SS losses, and an additional orthogonalisation of the predictions for the SS loss.

Dual-track representation. PETIMOT processes protein sequences through a message-passing neural network that simultaneously handles residue embeddings and motion vectors in local coordinate frames (Fig. 1). For each residue i, we define and update a node embedding $\mathbf{s}_i \in \mathbb{R}^d$ initialized from protein language model features and a set of K motion vectors $\{\vec{x}_{ik}\}_{k=1}^K \in \mathbb{R}^{3 \times K}$ initialized randomly. The message passing procedure is detailed in Algorithm B.1 of Appendix B.2. The

protein is represented as a graph where nodes correspond to the residues, and edges capture spatial relationships. We connect each residue i to its k nearest neighbors based on $C\alpha$ distances and l randomly selected residues. This hybrid connectivity scheme ensures both local geometric consistency and global information flow, while maintaining sparsity for computational efficiency. Indeed, our model scales linearly with the length N of a protein. In our base model we set k=5 and l=10.

Node and edge features. We chose ProstT5 as our default protein language model for initialising node embeddings (Heinzinger et al., 2023). This structure-aware pLM offers an excellent balance between model size – including the number of parameters and embedding dimensionality – and performance (Lombard et al., 2024b). Each residue's backbone atoms (N, CA, C) define a local reference frame through a rigid transformation $T_i \in SE(3)$. For each residue pair (i,j), we compute their relative transformation $T_{ij} = T_i^{-1} \circ T_j$ from which we extract the rotation $R_{ij} \in SO(3)$ and translation $\vec{t}_{ij} \in \mathbb{R}^3$. Under global rotations and translations of the protein, these relative transformations remain invariant. Edge features e_{ij} provide an SE(3)-invariant encoding of the protein structure through relative orientations, translational offsets, protein chain distance, and a complete description of peptide plane positioning captured by pairwise backbone atom distances. See Appendix B.3 for more details.

5 RESULTS

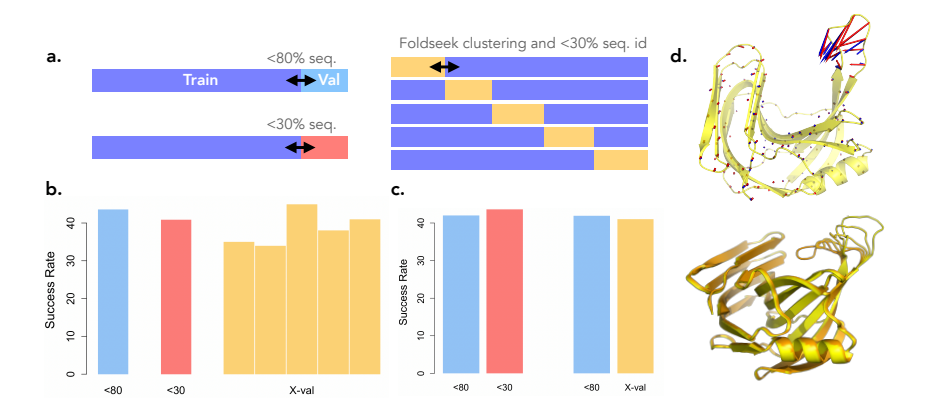


Figure 2: **Generalisation and prediction visualisation. a.** Training schemes. **b.** Success rates on the test sets for PETIMOT's default, stringent and 5folds models. **c.** Left: Comparison of the default and stringent models on 734 proteins with less than 30% sequence similarity to both models' training sets. Right: Comparison between default and 5folds on the 473 proteins whose structures and sequences are not significantly similar to any protein used in training the models. **d.** Prediction for *Bacillus subtilis* xylanase A (PDB id: 3EXU, chain A). On top, the predicted and ground-truth vectors are in blue and red, respectively (LS= 0.15). At the bottom, trajectory (5 frames) generated by deforming the protein structure along the predicted motion.

Training and evaluation. We trained PETIMOT against linear motions extracted from all \sim 750,000 protein chains from the PDB (as of June 2023) clustered at 80% sequence identity and coverage. Our full training data comprises 7 335 conformational collections, which we augmented by computing the motions with respect to 5 reference conformations per collection. As a result, the full training set comprises 36,675 samples. This reference dataset encompasses conformations solved by multiple experimental techniques, including 56,866 Cryo-EM structures (30.5%) and 2,187 NMR structures (about 1.5%). This ensures representation of diverse conformational states beyond those accessible to X-ray crystallography. We set the numbers of predicted and ground-truth motions, K = L = 4. See Appendices B.1 and B.4 for more details. At inference, we consider $w_i = 1$, $\forall i = 1...N$. We rely on three main evaluation metrics aimed at addressing the following questions: 1) Is PETIMOT able to approximate at least one of the main linear motions of a given protein? For this, we rely on the minimum LS error over all possible pairs of predicted and ground-truth vectors. A prediction with LS \leq 0.2 almost perfectly superimposes to the ground-truth motion (Fig. 2d). We consider predictions

with LS> 0.6 as inaccurate as they typically miss or indicate completely wrong directions for a large part of the residues involved in the motion. By comparison, the LS errors computed for random predictions are typically above 0.9; **2**) To what extent does PETIMOT capture the main motion linear subspace of a given protein? For this, we use the global SS error; **3**) Is PETIMOT able to identify the residues that move the most? Here, we rely on the magnitude error, $\frac{1}{N}\sum_{i=1}^{N}(\|\vec{y}_{ik}\|^2 - \|c_{kl}\vec{x}_{il}\|^2)$.

Robustness and generalisation. We tested PETIMOT's generalisation capabilities using three training protocols (Fig. 2a, see also Appendix B.4). In two of them, we randomly split the reference dataset into 70% for training, 15% for validation and 15% for test, where any test protein has less than 80% (*default*) or 30% (*stringent*) sequence similarity to the train proteins. In addition, we conducted 5-fold cross-validation ensuring that each fold's training set did not contain any protein chain sharing significant structural or sequence similarity with the test set (5 folds). This protocol strictly prevents data leakage and provides robust evaluation across our complete dataset. PETIMOT's performance is robust and generalizable across the different data partitions, with success rates, defined as the fractions of test proteins with min LS \leq 0.6, in the 35-45% range (Fig. 2b-c).

Biological relevance. To assess the biological relevance of PETIMOT's predictions, we focused on three case studies, namely open-closed transitions, fold switches, and multi-state cryo-EM resolved structures. For open-closed transitions, we considered the well-established iMod benchmark (Lopéz-Blanco et al., 2011) comprising a couple of tens of proteins with a wide variety of motions (hinge, shear, allosteric, and complex motions) often associated with ligand or partner binding. PETIMOT-5folds predicted these transitions with high accuracy, achieving a 86% success rate with an average min LS error of 0.41 ± 0.18 , average min magnitude error 0.14 ± 0.07 . For fold switches, we compiled a dataset of six metamorphic proteins from (Wayment-Steele et al., 2023). PETIMOT-*Sfolds* achieved a success rate of 37% on these challenging cases, with a min LS error of 0.67 \pm 0.17, min magnitude error 0.25 ± 0.14 . Our approach performed particularly well on KaiB, also highlighted in (Wayment-Steele et al., 2023). The min LS error is 0.45 starting from the ground state (2QKEC) and 0.57 starting from the FS state (5JYTA). Finally, we considered the ATPase NSF whose experimental structures correspond to ATP/ADP-bound states and 20S supercomplex conformations from cryo-EM studies (Zhao et al., 2015; White et al., 2018). The functionally relevant motions involve large-amplitude rigid-body domain movements and loop rearrangements. The first linear PCA mode explains 57% of the variance and 4 modes are required to explain 90%. PETIMOT successfully captures this complex motion subspace with min LS error as low as 0.32 and global SS error of 0.30, demonstrating its ability to predict not just single motions but biologically meaningful motion subspaces.

Comparison with other methods. We primarily compare PETIMOT with the NMA, a cost-effective approach for predicting the motion directions energetically accessible to a protein 3D structure. On the whole dataset, PETIMOT outperformed the NMA according to all evaluation metrics (Table 1). PETIMOT produced acceptable predictions for almost 40% of the dataset while

Table 1: **Comparison of PETIMOT**'s performance with other methods. Left: PETIMOT-*5folds* is compared with the Normal Mode Analysis (NMA) on the full dataset (37k samples). Right: PETIMOT-*default* is compared with the AlphaFlow and the NMA on 824 test proteins it has not seen during training Min. stands for the best matching pair of predicted and ground-truth vectors. OLA refers to the optimal linear assignment between all predicted and ground-truth vectors. Arrows indicate whether higher (↑) or lower (↓) metrics values are better. Best results are shown in **bold**.

Metrics	PETIMOT	NMA	PETIMOT	AlphaFlow	NMA
Success Rate (%) ↑	38.98	24.40	43.57	31.80	24.88
Min. LS Error ↓ Min. Magnitude Error ↓	$\begin{array}{c} \textbf{0.64} \pm \textbf{0.20} \\ \textbf{0.23} \pm \textbf{0.12} \end{array}$	$0.72 \pm 0.20 \\ 0.27 \pm 0.14$	$\begin{array}{ c c c c c c c c c c c c c c c c c c c$	$\begin{array}{c} 0.68 \pm 0.21 \\ 0.24 \pm 0.12 \end{array}$	$0.72 \pm 0.20 \\ 0.27 \pm 0.14$
OLA LS Error ↓ OLA Magnitude Error ↓	$\begin{array}{c} \textbf{0.84} \pm \textbf{0.09} \\ \textbf{0.41} \pm \textbf{0.13} \end{array}$	0.88 ± 0.09 0.47 ± 0.15	$\begin{array}{ c c } \textbf{0.83} \pm \textbf{0.10} \\ \textbf{0.41} \pm \textbf{0.14} \end{array}$	0.86 ± 0.10 0.43 ± 0.14	0.88 ± 0.10 0.48 ± 0.15
Global SS Error ↓	$\textbf{0.75} \pm \textbf{0.13}$	0.79 ± 0.14	$\textbf{0.73} \pm \textbf{0.14}$	0.78 ± 0.14	0.79 ± 0.14

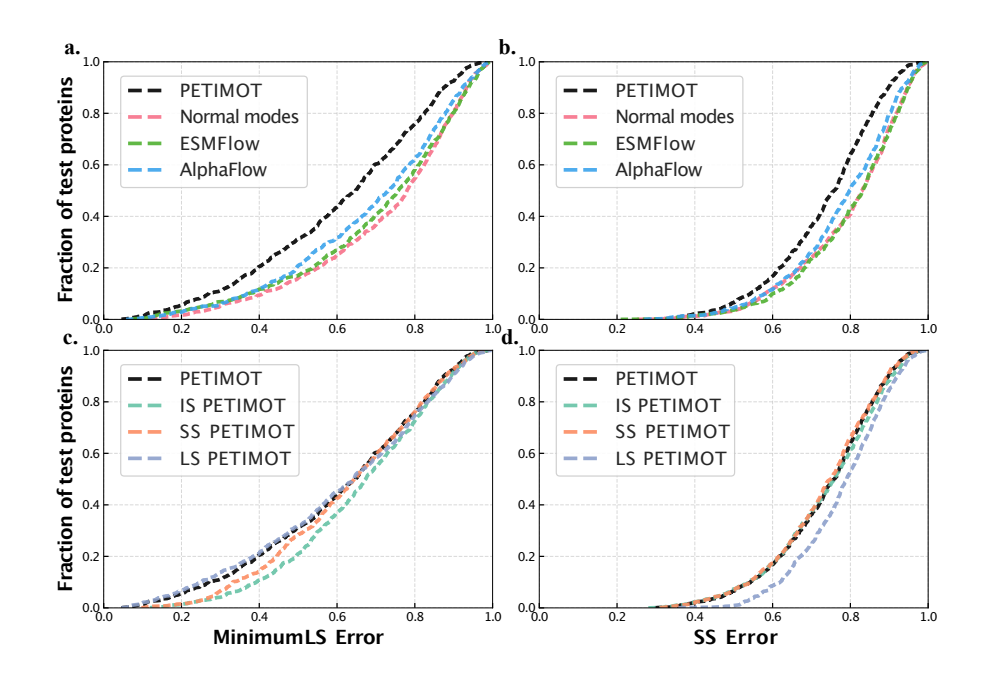


Figure 3: Cumulative error curves computed on the test proteins. a-b. Comparison between PETIMOT base model and three other methods. c-d. Comparison between different losses implemented in PETIMOT. The loss of the base model is LS + SS. a,c. Minimum LS error corresponding to the best matching pair of predicted and ground-truth motions. b,d. SS error computed between the entire predicted and ground-truth subspaces.

the NMA's success rate is 25%, and PETIMOT achieved lower errors than the NMA in two thirds of the proteins. The NMA success cases are enriched in collective motions and depleted in localised motions. PETIMOT does not share this limitation and tends to approximate localised motions better than the NMA. Furthermore, PETIMOT was 2.75 times faster at inference – 15.82s versus 43.59s on a subset of 800 proteins, as measured on an Intel(R) Xeon(R) W-2245 CPU @ 3.90GHz equipped with GeForce RTX 3090. In addition, we considered the flow matching-based AlphaFlow method, specifically the model trained solely on the PDB, like PETIMOT. However, AlphaFlow does not directly predict motion directions but generates conformational ensembles. We generated 50 conformations and estimated their distributional accuracy by extracting principal components and comparing them with our reference components, similarly to what was done in the AlphaFlow publication (Jing et al., 2024). On a test set of 824 proteins, PETIMOT-default better approximated the reference motions than AlphaFlow (Table 1 and Fig. 3a-b). The ESM-based version displayed slightly lower performance, compared to the AlphaFold-based one (Fig. 3a-b). PETIMOT min LS error is lower than AlphaFlow in 65% of the cases, than ESMFlow in 67% and than NMA in 69%. There are only 5, 4 and 2 cases, respectively, where PETIMOT produces highly inaccurate predictions (min LS loss above 0.7) and AlphaFlow, ESMFlow and the NMA, respectively, are clearly successful (min LS loss below 0.4). A couple of cases exhibit a highly localised loop motion (the peptidoglycan peptidase, 6JN8A, AlphaFlow better) or a rigid-body domain motion (the chromosomal replication initiator protein dnaA, 2HCBC, NMA better) involved in the function of the protein, but the majority exhibit large amplitude motions at the protein extremity, sometimes induced by insertions/deletions across the members of the collection, casting doubt on their functional relevance.

Comparison of problem formulations. Our base model combining the LS and SS loses with equal weights outperforms all three individual losses, LS, SS, and LS (Fig. 3c-d). It strikes an excellent balance between approximating individual motions with high accuracy (Fig. 3c) and globally covering the motion subspaces (Fig. 3d). By comparison, the SS and IS losses tend to underperform on individual motions while the LS loss tends to provide lower coverage of the ground-truth subspaces. See Appendix C for additional results.

Contribution of sequence and structure features. We performed an ablation study to assess the contribution of sequence and structure information to our architecture. Our results show that ProstT5 slightly outperforms the more recent and larger pLM, ESM-Cambrian 600M (ESM Team, 2024) (Fig. B.2). Geometrical information about protein structure provides the most significant contribution, as replacing ProstT5 embeddings with random numbers has only a small impact on network performance. Conversely, the network's performance without structural information strongly depends on the chosen pLM. While the structure-aware embeddings from ProstT5 partially compensate for missing 3D structure information, relying solely on ESM-C embeddings results in poor performance (Fig. B.2). Moreover, connecting each residue to its 15 nearest neighbours (sorted according to $C\alpha$ - $C\alpha$ distances) in the protein graph results in lower performance compared to introducing randomly chosen edges or even fully relying on random connectivity (Fig. B.4).

Generalisation to MD data. To further assess PETIMOT's robustness, we evaluated it on MD trajectories from the ATLAS dataset (Vander Meersche et al., 2024). We identified 400 protein chains common to both the ATLAS set and our dataset, providing an independent MD benchmark (see Appendix B.6). To ensure rigorous evaluation without data leakage, for each ATLAS protein chain we used the corresponding PETIMOT-folds model trained on the fold where that specific chain was held out from training (ensuring no training exposure). PETIMOT-5folds achieved a 60% success rate on this MD data – with a min LS error 0.55 ± 0.19 , min magnitude error 0.17 ± 0.11 , and global SS error 0.60 ± 0.16 . These performance metrics are significantly better than those obtained on experimental structures. Moreover, the association between min LS error and SS error is higher – Adjusted R-squared of 0.71 versus 0.60 on the PDB dataset (Fig. B.5). These results demonstrate that PETIMOT generalises to MD data without re-training nor fine-tuning.

Conformation generation. PETIMOT allows straightforwardly generating conformational ensembles or trajectories by deforming an initial protein 3D structure along one or a combination of predicted motions. We showcase this functionality on the xylanase A from *Bacillus subtilis* (Fig. 2d). We used PETIMOT predictions to generate physically realistic conformations representing the open-to-closed transition of xylanase A thumb. More broadly, PETIMOT-generated structures, while not being accurate in a thermodynamic sense, can help practitioners quickly assess possible dynamics or seed other workflows like heterogeneous cryo-EM reconstruction.

Limitations. PETIMOT's relatively modest success rate may be partially explained by incomplete and biased functional state sampling in the PDB, where predicted motions through evolutionary transfer may correspond to functionally relevant conformational states that have not been structurally resolved, and experimental artifacts (e.g., of crystallographic origin, or due to sequence engineering). Our working hypothesis is that a part of the conformational manifold represents functionally relevant motions. To address this challenge, we designed our training loss function specifically to evaluate submanifolds by calculating the minimum error between each reference motion and the set of predicted motions, allowing the model to capture conformational diversity while mitigating the impact of potential artefacts. By comparison, the Atlas MD trajectories represent an easier case but they are limited to equilibrium distributions of monomeric proteins and do not account for conformational changes induced by partner or ligand binding. In addition, our approach is limited to modeling protein motions as linear displacement vectors. While this approximation is sufficient to describe most of the observed conformational heterogeneity, it remains inadequate for modeling highly complex non-linear deformations. Furthermore, deforming proteins structures along linear motion direction may produce unrealistic conformations at large amplitudes. A possible solution yet to be investigated would be nonlinear extrapolation techniques widely used in molecular mechanics (Lopéz-Blanco et al., 2011; Hoffmann & Grudinin, 2017).

6 Conclusion

In this work, we have proposed a new perspective on the problem of capturing protein continuous conformational heterogeneity. Our approach directly infers compact and continuous representations of protein motions. Our comprehensive analysis of PETIMOT's predictive capabilities demonstrates its performance and utility for understanding how proteins deform to perform their functions. Our work opens ways to future developments in protein motion manifold learning, with exciting potential applications in protein engineering and drug development.

Ethics statement. This paper is about machine learning models for structural biology. The research is entirely computational and does not involve human subjects, animals, or sensitive data. All the data is public. We do not anticipate any direct societal, ethical, or environmental risks arising from this work.

Reproducibility statement. We ensure the reproducibility of this work through the following key points:

• Our code and protocols are available in an anonymous repository. We will share the link in the discussion forum.

• The problem formulation is provided in section 3 with the proofs in Appendix A.

• A complete description of the data processing steps is provided in Appendix B.1.

• The architecture and the training protocol are detailed in Appendices B.2, B.3, B.4.

 Evaluation procedures, and baselines' parameters are explained in Appendices B.4, B.5, B.6.

• Additional experiments and ablation studies are detailed in Appendices B.6 and C.

REFERENCES

Josh Abramson, Jonas Adler, Jack Dunger, Richard Evans, Tim Green, Alexander Pritzel, Olaf Ronneberger, Lindsay Willmore, Andrew J. Ballard, Joshua Bambrick, Sebastian W. Bodenstein, David A. Evans, Chia-Chun Hung, Michael O'Neill, David Reiman, Kathryn Tunyasuvunakool, Zachary Wu, Akvilė Žemgulytė, Eirini Arvaniti, Charles Beattie, Ottavia Bertolli, Alex Bridgland, Alexey Cherepanov, Miles Congreve, Alexander I. Cowen-Rivers, Andrew Cowie, Michael Figurnov, Fabian B. Fuchs, Hannah Gladman, Rishub Jain, Yousuf A. Khan, Caroline M. R. Low, Kuba Perlin, Anna Potapenko, Pascal Savy, Sukhdeep Singh, Adrian Stecula, Ashok Thillaisundaram, Catherine Tong, Sergei Yakneen, Ellen D. Zhong, Michal Zielinski, Augustin Žídek, Victor Bapst, Pushmeet Kohli, Max Jaderberg, Demis Hassabis, and John M. Jumper. Accurate structure prediction of biomolecular interactions with alphafold 3. *Nature*, 630(8016):493–500, 2024. doi: 10.1038/s41586-024-07487-w. URL https://doi.org/10.1038/s41586-024-07487-w.

Gustaf Ahdritz, Nazim Bouatta, Christina Floristean, Sachin Kadyan, Qinghui Xia, William Gerecke, Timothy J O'Donnell, Daniel Berenberg, Ian Fisk, Niccolò Zanichelli, et al. Openfold: Retraining alphafold2 yields new insights into its learning mechanisms and capacity for generalization. *Nature Methods*, 21(8):1514–1524, 2024.

Andrea Amadei, Marc A Ceruso, and Alfredo Di Nola. On the convergence of the conformational coordinates basis set obtained by the essential dynamics analysis of proteins' molecular dynamics simulations. *Proteins: Structure, Function, and Bioinformatics*, 36(4):419–424, 1999.

Zineb Belkacemi, Paraskevi Gkeka, Tony Lelièvre, and Gabriel Stoltz. Chasing collective variables using autoencoders and biased trajectories. *Journal of chemical theory and computation*, 18(1): 59–78, 2021.

Helen M Berman, John Westbrook, Zukang Feng, Gary Gilliland, Talapady N Bhat, Helge Weissig, Ilya N Shindyalov, and Philip E Bourne. The protein data bank. *Nucleic acids research*, 28(1): 235–242, 2000.

Robert B Best, Kresten Lindorff-Larsen, Mark A DePristo, and Michele Vendruscolo. Relation between native ensembles and experimental structures of proteins. *Proceedings of the National Academy of Sciences*, 103(29):10901–10906, 2006.

Luigi Bonati, GiovanniMaria Piccini, and Michele Parrinello. Deep learning the slow modes for rare events sampling. *Proceedings of the National Academy of Sciences*, 118(44):e2113533118, 2021.

Patrick Bryant and Frank Noé. Structure prediction of alternative protein conformations. *Nature Communications*, 15(1):7328, 2024.

- Devlina Chakravarty, Myeongsang Lee, and Lauren L Porter. Proteins with alternative folds reveal blind spots in alphafold-based protein structure prediction. *Current Opinion in Structural Biology*, 90:102973, 2025.
 - Haochuan Chen, Benoît Roux, and Christophe Chipot. Discovering reaction pathways, slow variables, and committor probabilities with machine learning. *Journal of Chemical Theory and Computation*, 19(14):4414–4426, 2023a.
 - Wei Chen, Zichen Miao, and Qiang Qiu. Inner product-based neural network similarity. *Advances in Neural Information Processing Systems*, 36:73995–74020, 2023b.
 - Justas Dauparas, Ivan Anishchenko, Nathaniel Bennett, Hua Bai, Robert J Ragotte, Lukas F Milles, Basile IM Wicky, Alexis Courbet, Rob J de Haas, Neville Bethel, et al. Robust deep learning–based protein sequence design using proteinmpnn. *Science*, 378(6615):49–56, 2022.
 - Charles C David and Donald J Jacobs. Characterizing protein motions from structure. *Journal of Molecular Graphics and Modelling*, 31:41–56, 2011.
 - Diego Del Alamo, Davide Sala, Hassane S Mchaourab, and Jens Meiler. Sampling alternative conformational states of transporters and receptors with alphafold2. *Elife*, 11:e75751, 2022.
 - . ESM Team. Esm cambrian: Revealing the mysteries of proteins with unsupervised learning. Evolutionary Scale Website, 2024. URL https://evolutionaryscale.ai/blog/esm-cambrian. Available from: https://evolutionaryscale.ai/blog/esm-cambrian.
 - Bulat Faezov and Roland L Dunbrack Jr. Alphafold2 models of the active form of all 437 catalytically-competent typical human kinase domains. *bioRxiv*, pp. 2023–07, 2023.
 - Qizhang Feng, Zhimeng Stephen Jiang, Ruiquan Li, Yicheng Wang, Na Zou, Jiang Bian, and Xia Hu. Fair graph distillation. *Advances in Neural Information Processing Systems*, 36:80644–80660, 2023.
 - Sergei Grudinin, Elodie Laine, and Alexandre Hoffmann. Predicting protein functional motions: an old recipe with a new twist. *Biophysical journal*, 118(10):2513–2525, 2020.
 - Sam Hawke, YueEn Ma, and Didong Li. Contrastive dimension reduction: when and how? *Advances in Neural Information Processing Systems*, 37:74034–74057, 2024.
 - Thomas Hayes, Roshan Rao, Halil Akin, Nicholas J. Sofroniew, Deniz Oktay, Zeming Lin, Robert Verkuil, Vincent Q. Tran, Jonathan Deaton, Marius Wiggert, Rohil Badkundri, Irhum Shafkat, Jun Gong, Alexander Derry, Raul S. Molina, Neil Thomas, Yousuf Khan, Chetan Mishra, Carolyn Kim, Liam J. Bartie, Matthew Nemeth, Patrick D. Hsu, Tom Sercu, Salvatore Candido, and Alexander Rives. Simulating 500 million years of evolution with a language model. bioRxiv, 2024. doi: 10.1101/2024.07.01.600583. URL https://www.biorxiv.org/content/early/2024/07/02/2024.07.01.600583.
 - Steven Hayward and Nobuhiro Go. Collective variable description of native protein dynamics. *Annual review of physical chemistry*, 46(1):223–250, 1995.
 - Michael Heinzinger, Konstantin Weissenow, Joaquin Gomez Sanchez, Adrian Henkel, Martin Steinegger, and Burkhard Rost. Prostt5: Bilingual language model for protein sequence and structure. *bioRxiv*, pp. 2023–07, 2023.
 - Lim Heo and Michael Feig. Multi-state modeling of g-protein coupled receptors at experimental accuracy. *Proteins: Structure, Function, and Bioinformatics*, 90(11):1873–1885, 2022.
 - Alexandre Hoffmann and Sergei Grudinin. Nolb: Nonlinear rigid block normal-mode analysis method. *Journal of chemical theory and computation*, 13(5):2123–2134, 2017.
 - John Ingraham, Vikas Garg, Regina Barzilay, and Tommi Jaakkola. Generative models for graph-based protein design. *Advances in neural information processing systems*, 32, 2019.

- John B Ingraham, Max Baranov, Zak Costello, Karl W Barber, Wujie Wang, Ahmed Ismail, Vincent Frappier, Dana M Lord, Christopher Ng-Thow-Hing, Erik R Van Vlack, et al. Illuminating protein space with a programmable generative model. *Nature*, 623(7989):1070–1078, 2023.
 - Bowen Jing, Stephan Eismann, Patricia Suriana, Raphael JL Townshend, and Ron Dror. Learning from protein structure with geometric vector perceptrons. *arXiv preprint arXiv:2009.01411*, 2020.
 - Bowen Jing, Ezra Erives, Peter Pao-Huang, Gabriele Corso, Bonnie Berger, and Tommi Jaakkola. Eigenfold: Generative protein structure prediction with diffusion models. *arXiv preprint arXiv:2304.02198*, 2023.
 - Bowen Jing, Bonnie Berger, and Tommi Jaakkola. Alphafold meets flow matching for generating protein ensembles. *arXiv preprint arXiv:2402.04845*, 2024.
 - Robbie P Joosten, Fei Long, Garib N Murshudov, and Anastassis Perrakis. The pdb_redo server for macromolecular structure model optimization. *IUCrJ*, 1(4):213–220, 2014.
 - John Jumper, Richard Evans, Alexander Pritzel, Tim Green, Michael Figurnov, Olaf Ronneberger, Kathryn Tunyasuvunakool, Russ Bates, Augustin Žídek, Anna Potapenko, Alex Bridgland, Clemens Meyer, Simon A. A. Kohl, Andrew J. Ballard, Andrew Cowie, Bernardino Romera-Paredes, Stanislav Nikolov, Rishub Jain, Jonas Adler, Trevor Back, Stig Petersen, David Reiman, Ellen Clancy, Michal Zielinski, Martin Steinegger, Michalina Pacholska, Tamas Berghammer, Sebastian Bodenstein, David Silver, Oriol Vinyals, Andrew W. Senior, Koray Kavukcuoglu, Pushmeet Kohli, and Demis Hassabis. Highly accurate protein structure prediction with alphafold. *Nature*, 596(7873):583–589, 2021. doi: 10.1038/s41586-021-03819-2. URL https://doi.org/10.1038/s41586-021-03819-2.
 - W. Kabsch. A solution for the best rotation to relate two sets of vectors. *Acta Crystallographica Section A*, 32(5):922–923, Sep 1976. doi: 10.1107/S0567739476001873. URL https://doi.org/10.1107/S0567739476001873.
 - Yogesh Kalakoti and Björn Wallner. Afsample2: Predicting multiple conformations and ensembles with alphafold2. *bioRxiv*, pp. 2024–05, 2024.
 - Simon K Kearsley. On the orthogonal transformation used for structural comparisons. *Acta Crystallographica Section A: Foundations of Crystallography*, 45(2):208–210, 1989.
 - Leon Klein, Andrew Foong, Tor Fjelde, Bruno Mlodozeniec, Marc Brockschmidt, Sebastian Nowozin, Frank Noé, and Ryota Tomioka. Timewarp: Transferable acceleration of molecular dynamics by learning time-coarsened dynamics. *Advances in Neural Information Processing Systems*, 36, 2024.
 - Lucien F Krapp, Luciano A Abriata, Fabio Cortés Rodriguez, and Matteo Dal Peraro. Pesto: parameter-free geometric deep learning for accurate prediction of protein binding interfaces. *Nature communications*, 14(1):2175, 2023.
 - Rohith Krishna, Jue Wang, Woody Ahern, Pascal Sturmfels, Preetham Venkatesh, Indrek Kalvet, Gyu Rie Lee, Felix S Morey-Burrows, Ivan Anishchenko, Ian R Humphreys, et al. Generalized biomolecular modeling and design with rosettafold all-atom. *Science*, 384(6693):eadl2528, 2024.
 - Elodie Laine and Sergei Grudinin. Hopma: Boosting protein functional dynamics with colored contact maps. *The Journal of Physical Chemistry B*, 125(10):2577–2588, 2021.
 - Thomas J Lane. Protein structure prediction has reached the single-structure frontier. *Nature Methods*, 20(2):170–173, 2023.
- Alejandra Leo-Macias, Pedro Lopez-Romero, Dmitry Lupyan, Daniel Zerbino, and Angel R Ortiz.
 An analysis of core deformations in protein superfamilies. *Biophysical journal*, 88(2):1291–1299, 2005.
 - Sarah Lewis, Tim Hempel, José Jiménez-Luna, Michael Gastegger, Yu Xie, Andrew YK Foong, Victor García Satorras, Osama Abdin, Bastiaan S Veeling, Iryna Zaporozhets, et al. Scalable emulation of protein equilibrium ensembles with generative deep learning. *Science*, 389(6761): eadv9817, 2025.

- Zeming Lin, Halil Akin, Roshan Rao, Brian Hie, Zhongkai Zhu, Wenting Lu, Nikita Smetanin, Robert Verkuil, Ori Kabeli, Yaniv Shmueli, Allan Dos Santos Costa, Maryam Fazel-Zarandi, Tom Sercu, Salvatore Candido, and Alexander Rives. Evolutionary-scale prediction of atomic-level protein structure with a language model. *Science*, 379(6637):1123–1130, 2023.
 - Junqi Liu, Shaoning Li, Chence Shi, Zhi Yang, and Jian Tang. Design of ligand-binding proteins with atomic flow matching. *arXiv preprint arXiv:2409.12080*, 2024.
 - Valentin Lombard, Sergei Grudinin, and Elodie Laine. Explaining conformational diversity in protein families through molecular motions. *Scientific Data*, 11(1):752, 2024a.
 - Valentin Lombard, Dan Timsit, Sergei Grudinin, and Elodie Laine. Seamoon: Prediction of molecular motions based on language models. *bioRxiv*, pp. 2024–09, 2024b.
 - José Ramón Lopéz-Blanco, José Ignacio Garzón, and Pablo Chacón. imod: multipurpose normal mode analysis in internal coordinates. *Bioinformatics*, 27(20):2843–2850, 2011.
 - Ilya Loshchilov and Frank Hutter. Decoupled weight decay regularization. In *International Conference on Learning Representations*, 2019. URL https://openreview.net/forum?id=Bkq6RiCqY7.
 - Frank Noé, Simon Olsson, Jonas Köhler, and Hao Wu. Boltzmann generators: Sampling equilibrium states of many-body systems with deep learning. *Science*, 365(6457):eaaw1147, 2019.
 - Lauren L Porter, Irina Artsimovitch, and César A Ramírez-Sarmiento. Metamorphic proteins and how to find them. *Current opinion in structural biology*, 86:102807, 2024.
 - Venkata K Ramaswamy, Samuel C Musson, Chris G Willcocks, and Matteo T Degiacomi. Deep learning protein conformational space with convolutions and latent interpolations. *Physical Review X*, 11(1):011052, 2021.
 - Nessim Raouraoua, Claudio Mirabello, Thibaut Véry, Christophe Blanchet, Björn Wallner, Marc F. Lensink, and Guillaume Brysbaert. MassiveFold: unveiling AlphaFold's hidden potential with optimized and parallelized massive sampling. *Nature Computational Science*, 4(11): 824–828, 2024. doi: 10.1038/s43588-024-00714-4. URL https://doi.org/10.1038/s43588-024-00714-4.
 - João Marcelo Lamim Ribeiro, Pablo Bravo, Yihang Wang, and Pratyush Tiwary. Reweighted autoencoded variational bayes for enhanced sampling (rave). The Journal of chemical physics, 149 (7), 2018.
 - Tadeo Saldaño, Nahuel Escobedo, Julia Marchetti, Diego Javier Zea, Juan Mac Donagh, Ana Julia Velez Rueda, Eduardo Gonik, Agustina García Melani, Julieta Novomisky Nechcoff, Martín N Salas, et al. Impact of protein conformational diversity on alphafold predictions. *Bioinformatics*, 38(10):2742–2748, 2022.
 - Andreas Schlaginhaufen and Maryam Kamgarpour. Towards the transferability of rewards recovered via regularized inverse reinforcement learning. *Advances in Neural Information Processing Systems*, 37:21461–21501, 2024.
 - Melanie Schneider, José Antonio Marquez, and Andrew R. Leach. Ensembleflex: Protein structure ensemble analysis made easy. *Structure*, 2025. ISSN 0969-2126. doi: https://doi.org/10.1016/j.str.2025.07.001. URL https://www.sciencedirect.com/science/article/pii/S0969212625002497.
 - Richard A Stein and Hassane S Mchaourab. Speach_af: Sampling protein ensembles and conformational heterogeneity with alphafold2. *PLOS Computational Biology*, 18(8):e1010483, 2022.
 - Martin Steinegger and Johannes Söding. Mmseqs2 enables sensitive protein sequence searching for the analysis of massive data sets. *Nature Biotechnology*, 35(11):1026–1028, Nov 2017. ISSN 1546-1696. doi: 10.1038/nbt.3988. URL https://doi.org/10.1038/nbt.3988.

- Michel Van Kempen, Stephanie S Kim, Charlotte Tumescheit, Milot Mirdita, Jeongjae Lee, Cameron LM Gilchrist, Johannes Söding, and Martin Steinegger. Fast and accurate protein structure search with foldseek. *Nature biotechnology*, 42(2):243–246, 2024.
 - Yann Vander Meersche, Gabriel Cretin, Aria Gheeraert, Jean-Christophe Gelly, and Tatiana Galochkina. Atlas: protein flexibility description from atomistic molecular dynamics simulations. *Nucleic acids research*, 52(D1):D384–D392, 2024.
 - Mihaly Varadi, Damian Bertoni, Paulyna Magana, Urmila Paramval, Ivanna Pidruchna, Malarvizhi Radhakrishnan, Maxim Tsenkov, Sreenath Nair, Milot Mirdita, Jingi Yeo, et al. Alphafold protein structure database in 2024: providing structure coverage for over 214 million protein sequences. *Nucleic acids research*, 52(D1):D368–D375, 2024.
 - Björn Wallner. Afsample: improving multimer prediction with alphafold using massive sampling. *Bioinformatics*, 39(9):btad573, 2023.
 - Tong Wang, Xinheng He, Mingyu Li, Yatao Li, Ran Bi, Yusong Wang, Chaoran Cheng, Xiangzhen Shen, Jiawei Meng, He Zhang, et al. Ab initio characterization of protein molecular dynamics with ai2bmd. *Nature*, pp. 1–9, 2024a.
 - Y Wang, L Wang, Y Shen, Y Wang, H Yuan, Y Wu, and Q Gu. Protein conformation generation via force-guided se (3) diffusion models, 2024. doi: 10.48550. arXiv preprint ARXIV.2403.14088, 2025.
 - Yihang Wang, Joao Marcelo Lamim Ribeiro, and Pratyush Tiwary. Machine learning approaches for analyzing and enhancing molecular dynamics simulations. *Current opinion in structural biology*, 61:139–145, 2020.
 - Yusong Wang, Tong Wang, Shaoning Li, Xinheng He, Mingyu Li, Zun Wang, Nanning Zheng, Bin Shao, and Tie-Yan Liu. Enhancing geometric representations for molecules with equivariant vector-scalar interactive message passing. *Nature Communications*, 15(1):313, 2024b.
 - Hannah K Wayment-Steele, Adedolapo Ojoawo, Renee Otten, Julia M Apitz, Warintra Pitsawong, Marc Hömberger, Sergey Ovchinnikov, Lucy Colwell, and Dorothee Kern. Predicting multiple conformations via sequence clustering and alphafold2. *Nature*, pp. 1–3, 2023.
 - Konstantin Weissenow, Michael Heinzinger, and Burkhard Rost. Protein language-model embeddings for fast, accurate, and alignment-free protein structure prediction. *Structure*, 30(8):1169–1177, 2022.
 - K Ian White, Minglei Zhao, Ucheor B Choi, Richard A Pfuetzner, and Axel T Brunger. Structural principles of snare complex recognition by the aaa+ protein nsf. *Elife*, 7:e38888, 2018.
 - Ruidong Wu, Fan Ding, Rui Wang, Rui Shen, Xiwen Zhang, Shitong Luo, Chenpeng Su, Zuofan Wu, Qi Xie, Bonnie Berger, et al. High-resolution de novo structure prediction from primary sequence. *BioRxiv*, pp. 2022–07, 2022.
 - Lee-Wei Yang, Eran Eyal, Ivet Bahar, and Akio Kitao. Principal component analysis of native ensembles of biomolecular structures (pca_nest): insights into functional dynamics. *Bioinformatics*, 25(5):606–614, 2009.
 - Zongxin Yu, Yikai Liu, Guang Lin, Wen Jiang, and Ming Chen. ESMAdam: a plug-and-play all-purpose protein ensemble generator. *bioRxiv*, pp. 2025–01, 2025.
 - Yang Zhang and Jeffrey Skolnick. Tm-align: a protein structure alignment algorithm based on the tm-score. *Nucleic acids research*, 33(7):2302–2309, 2005.
 - Minglei Zhao, Shenping Wu, Qiangjun Zhou, Sandro Vivona, Daniel J Cipriano, Yifan Cheng, and Axel T Brunger. Mechanistic insights into the recycling machine of the snare complex. *Nature*, 518(7537):61–67, 2015.

Shuxin Zheng, Jiyan He, Chang Liu, Yu Shi, Ziheng Lu, Weitao Feng, Fusong Ju, Jiaxi Wang, Jianwei Zhu, Yaosen Min, He Zhang, Shidi Tang, Hongxia Hao, Peiran Jin, Chi Chen, Frank Noé, Haiguang Liu, and Tie-Yan Liu. Predicting equilibrium distributions for molecular systems with deep learning. *Nature Machine Intelligence*, 6(5):558–567, 2024. doi: 10.1038/s42256-024-00837-3. URL https://doi.org/10.1038/s42256-024-00837-3.

Fei Zhu, Zhen Cheng, Xu-Yao Zhang, and Cheng-lin Liu. Class-incremental learning via dual augmentation. *Advances in neural information processing systems*, 34:14306–14318, 2021.

APPENDICES

A INVARIANCE OF THE PROPOSED LOSSES

Theorem A.1. SS Loss is invariant under unitary transformations of X and Y subspaces.

Proof. Without loss of generality, let us assume that we apply a unitary transformation $U \in \mathbb{R}^{K \times K}$ to a subspace $X^{\perp} \in \mathbb{R}^{3N \times K}$, such that the result $X' = X^{\perp}U$, with $X' \in \mathbb{R}^{3N \times K}$, spans the same subspace as X^{\perp} , as it is a linear combination of the original basis vectors from X^{\perp} . Then, let us rewrite the SS loss as

SS Loss =
$$1 - \frac{1}{K} \sum_{k=1}^{K} \sum_{l=1}^{K} (\mathbf{y}_k^T W^{\frac{1}{2}} \mathbf{x}_l^{\perp})^2 = 1 - \frac{1}{K} ||Y^T W^{\frac{1}{2}} X^{\perp}||_F^2.$$
 (A.1)

As the Frobenius matrix norm is invariant under orthogonal, or more generally, unitary, transformations, $||Y^TW^{\frac{1}{2}}X^{\perp}U||_F^2 = ||Y^TW^{\frac{1}{2}}X^{\perp}||_F^2$, which completes the proof.

Corollary A.1.1. The SS loss is invariant to the direction permutations in the Gram-Schmidt orthogonalization process.

Proof. Let us consider two linear subspaces X_1^\perp and X_2^\perp resulting from the Gram-Schmidt orthogonalization of X, where we arbitrarily choose the order of the orthogonalization vectors. Both X_1^\perp and X_2^\perp will span the same subspace as X, and since both X_1^\perp and X_2^\perp are also orthogonal, one is a unitary transformation of the other, $X_2^\perp = X_1^\perp U$, which completes the proof.

Theorem A.2. IS Loss is invariant under unitary transformations of X and Y subspaces.

Proof. Following the previous proof, without loss of generality, let us assume that we apply an orthogonal (unitary) transformation $U \in \mathbb{R}^{K \times K}$ to a subspace $X \in \mathbb{R}^{3N \times K}$, such that the result X' = XU, with $X' \in \mathbb{R}^{3N \times K}$, spans the same subspace as X. Then, let us rewrite the IS loss as

IS Loss =
$$\frac{1}{K^2} \sum_{k=1}^{K} \sum_{l=1}^{K} (\mathbf{x}_k^T W \mathbf{x}_l)^2 - \frac{1}{K^2} \sum_{k=1}^{K} \sum_{l=1}^{K} (\mathbf{y}_k^T W^{\frac{1}{2}} \mathbf{x}_l)^2 = \frac{1}{K^2} ||X^T W X||_F^2 - \frac{1}{K^2} ||Y^T W^{\frac{1}{2}} X||_F^2.$$
(A.2)

As the Frobenius matrix norm is invariant under orthogonal transformations, $||Y^TW^{\frac{1}{2}}XU||_F^2 = ||Y^TW^{\frac{1}{2}}X||_F^2$, and $||U^TX^TWXU||_F^2 = ||X^TWX||_F^2$, which completes the proof.

B METHODS DETAILS

B.1 TRAINING DATA

Conformational collections. To generate the training data, we utilized DANCE (Lombard et al., 2024a) to construct a non-redundant set of conformational collections representing the entire PDB as of June 2023. Wherever possible, we enhanced the data quality by replacing raw PDB coordinates with their updated and optimized counterparts from PDB-REDO (Joosten et al., 2014). Each conformational collection was designed to include only closely related homologs, ensuring that any two protein chains within the same collection shared at least 80% sequence identity and coverage. Collections with insufficient data points were excluded as we require at least 5 conformations. To simplify the data, we retained only $C\alpha$ atoms (option -c) and accounted for coordinate uncertainty by applying weights (option -w).

Handling missing data. The conformations in a collection may have different lengths reflected by the introduction of gaps when aligning the amino acid sequences. We fill these gaps with the coordinates of the conformation used to center the data. In doing so, we avoid introducing biases through reconstruction of the missing coordinates. Moreover, to explicitly account for data uncertainty,

we assign confidence scores to the residues and include them in the structural alignment step and the eigen decomposition. The confidence score of a position i reflects its coverage in the alignment,

$$w_i = \frac{1}{m} \sum_{S} \mathbb{1}_{a_i^S \neq \text{"X"}},$$
 (B.1)

where "X" is the symbol used for gaps and m is the number of conformations. The structural alignment of the jth conformation onto the reference conformation amounts to determining the optimal rotation that minimises the following function (Kabsch, 1976; Kearsley, 1989),

$$E = \frac{1}{\sum_{i} w_{i}} \sum_{i} w_{i} (r_{ij}^{c} - r_{i0}^{c})^{2},$$
(B.2)

where r_{ij}^c is the *i*th centred coordinate of the *j*th conformation and r_{i0}^c is the *i*th centred coordinate of the reference conformation. The resulting aligned coordinates are then multiplied by the confidence scores prior to the PCA, as we explain below.

Eigenspaces of positional covariance matrices. The Cartesian coordinates of each conformational ensemble can be stored in a matrix R of dimension $3N \times m$, where N is the number of residues (or positions in the associated multiple sequence alignment) and n is the number of conformations. Each position is represented by a C- α atom. We compute the coverage-weighted (to account for missing data, as explained above) covariance matrix as in Eq. 2. The covariance matrix is a $3N \times 3N$ square matrix, symmetric and real.

We decompose C as $C = VDV^T$, where V is a $3N \times 3N$ matrix with each column defining a sqrt-coverage-weighted eigenvector or a principal component that we interpret as a *linear motion*. D is a diagonal matrix containing the eigenvalues. Specifically, the kth principal component was expressed as a set of 3D (sqrt-coverage-weighted) displacement vectors \vec{x}_{ik}^{GT} , i=1,2,...L for the L $C\alpha$ atoms of the protein residues. To enable cross-protein comparisons, the vectors were normalized such that $\sum i = 1^L |\vec{x}_{ik}^{GT}|^2 = L$. The sum of the eigenvalues $\sum_{k=1}^{3m} \lambda_k$ amounts to the total positional variance of the ensemble (measured in Ų) and each eigenvalue reflects the amount of variance explained by the associated eigenvector.

Data augmentation. The reference conformation used to align and center the 3D coordinates corresponds to the protein chain with the most representative amino acid sequence. To increase data diversity, four additional reference conformations were defined for each collection. At each iteration, the new reference conformation was selected as the one with the highest RMSD relative to the previous reference. This iterative strategy maximizes the variability of the extracted motions by emphasizing the impact of changing the reference.

B.2 MESSAGE PASSING

The node embeddings and predicted motion vectors are updated iteratively according to the following algorithm.

Algorithm B.1 PETIMOT Message Passing Block

918

919

920

921

922

923

924

925

926

927

928

929

930

931

932

933

934 935 936

937 938

939

940

941

942

943

944

945 946

947 948

949

950

951

953

954

955

956

957

958

959 960

961

962 963

964 965

966

967

968

969

970

971

```
1: function MESSAGEPASSING(\{\mathbf{s}_i\}, \{\vec{x}_i\}, \{\mathcal{N}eigh(i)\}, \{R_{ij}, e_{ij}\}):
    2: \{\mathbf{s}_i\}_{i=1}^N
3: \{\vec{x}_i\}_{i=1}^N

    Node embeddings
    Node embeddings

                                                                                                                                                                                                                                                                                                                                                          ▶ Motion vectors in local frames
     4: # \{Neigh(i)\}_{i=1}^{N}

    Node neighborhoods

    5: # \{R_{ij}, e_{ij}\}
                                                                                                                                                                                                                                                                                                                                                                          ▶ Relative geometric features
                                        for i=1 to N do
    7:
                                                           for j \in \mathcal{N}eigh(i) do
                                                                                                                                                                                                                                                                                                                                                                                     \triangleright Project motion in frame i
    8:
                                                                                \vec{x}_i^i \leftarrow R_{ij}\vec{x}_j
                                                                              m_{ij} \leftarrow \text{MessageMLP}(\mathbf{s}_i, \mathbf{s}_j, \vec{x}_i, \vec{x}_i^i, e_{ij})
    9:
10:
                                                           m_i \leftarrow \mathrm{Mean}_i(m_{ij})
11:
                                                                                                                                                                                                                                                                                                                                                                                                              12:
                                                           \mathbf{s}_i \leftarrow \mathbf{s}_i + \text{LayerNorm}(m_i)
                                                                                                                                                                                                                                                                                                                                                                                                                      ▶ Update embedding
                                                            \vec{x}_i \leftarrow \vec{x}_i + \text{Linear}([\mathbf{s}_i, \vec{x}_i])
13:
                                                                                                                                                                                                                                                                                                                                                                                                                                            ▶ Update motion
14:
                                        return \{\mathbf{s}_i\}_{i=1}^N, \{\vec{x}_i\}_{i=1}^N
15:
16: end function
```

B.3 SE(3)-EQUIVARIANT FEATURES

We represent protein structures as attributed graphs. The node embeddings are computed with the pre-trained protein language model ProstT5 (Heinzinger et al., 2023). It is a fine-tuned version of the sequence-only model T5 that translates amino acid sequences into sequences of discrete structural states and reciprocally.

The edge embeddings are computed using SE(3)-invariant features derived from the input backbone, similarly to prior works (Ingraham et al., 2023; Dauparas et al., 2022; Ingraham et al., 2019). Specifically, the features associated with the edge e_{ij} from node (atom) i to node (atom) j are:

- Quaternion representation: A 4-dimensional quaternion encoding the relative rotation R_{ij} between the local reference frames of residues i and j.
- **Relative translation:** A 3-dimensional vector representing the translation \vec{t}_{ij} between the local reference frames.
- Chain separation: The sequence separation between residues i and j, encoded as $\log(|i-j|+1)$.
- Spatial separation: The logarithm of the Euclidean distance between residues i and j, computed as $\log(\|\vec{t}_{ij}\| + \epsilon)$, where $\epsilon = 10^{-8}$.
- Backbone atoms distances: Distances between all backbone atoms (N, $C\alpha$, C, O) at residues i and j, encoded through a radial basis expansion. For each pairwise distance d_{ab} , we compute:

$$f_k(d_{ab}) = \exp\left(-\frac{(d_{ab} - \mu_k)^2}{2\sigma^2}\right),\tag{B.3}$$

where $\{\mu_k\}_{k=1}^{20}$ are centers spaced linearly in [0,20] Å and $\sigma=1$ Å. This creates a $16\times 20=320$ dimensional feature vector, as we have 16 pairwise distances (4 × 4 atoms) each expanded in 20 basis functions.

B.4 TRAINING PROCEDURE

For the *default* version, we randomly split the 7,335 conformational collections defined with DANCE into training, validation, and test sets with a ratio 70:15:15. The data augmentation procedure resulted in $5,119 \times 5 = 25,595$ training samples and $1,099 \times 5 = 5,495$ validation samples.

For the *stringent* version, we considered clusters of protein chains defined at 30% sequence identity and 80% sequence coverage using MMseqs2 (Steinegger & Söding, 2017). These clusters define distant protein families and we refer to them as clus-30 in the following. We kept the test proteins used PETIMOT-*default* as is and we removed all collections belonging to the same clus-30 clusters

as these proteins from the training and validation sets. Then, we re-defined a training-validation random split at the level of the clus-30 clusters with a 9:1 ratio. This operation ensures that any pair of training-validation, training-test or validation-test collections do not share more than 30% sequence identity. Finally, for each training or validation clus-30 cluster, we randomly drew 5 samples. This step ensures that each protein family is evenly represented in the training and validation sets.

For the *5fold* version, we conducted a 5-fold cross-validation experiment with strict similarity filtering. We ensured a two-stage similarity filtering process:

- 1. **Structural similarity removal:** First, we used FoldSeek (Van Kempen et al., 2024) to cluster protein chains using an e-value threshold of 1e-2. Any two chains belonging to two different clusters do not share significant structural similarity.
- 2. **Sequential similarity removal:** We randomly partitioned the dataset into 5 folds and applied a cross-validation procedure. We implemented an additional sequence similarity-based filtering using MMseqs2. Specifically, for each fold, we removed from the training set (80% of the data) the protein chains sharing more than 30% sequence identity with any of the chains from the test set (20%).

The models were optimized using AdamW (Loshchilov & Hutter, 2019) with a learning rate of 5e-4 and weight decay of 0.01. We employed gradient clipping with a maximum norm of 10.0 and mixed precision training with PyTorch's Automatic Mixed Precision. The learning rate was adjusted using torch's ReduceLROnPlateau scheduler, which monitored the validation loss, reducing the learning rate by a factor of 0.2 after 10 epochs without improvement. Training was performed with a batch size of 32 for both training and validation sets. We implemented early stopping with a patience of 50 epochs, monitoring the validation loss. The model achieving the best validation performance was selected for final evaluation. We trained the model on a single NVIDIA A100-SXM4-80GB GPU. One epoch took about 9 minutes of real time.

Comparison with the Normal Mode Analysis. We compared our approach with the physics-based unsupervised Normal Mode Analysis (NMA) method (Hayward & Go, 1995). The NMA takes as input a protein 3D structure and builds an elastic network model where the nodes represent the atoms and the edges represent springs linking atoms located close to each other in 3D space. The four lowest normal modes are obtained by diagonalizing the mass-weighted Hessian matrix of the potential energy of this network. We used the highly efficient NOLB method, version 1.9, downloaded from https://team.inria.fr/nano-d/software/nolb-normal-modes/ (Hoffmann & Grudinin, 2017) to extract the first K normal modes from the test protein 3D conformations. Specifically, we used the following command

```
NOLB INPUT.pdb -c 10 -x -n 4 --linear -s 0 --format 1 --hetatm
```

We retained only the $C\alpha$ atoms and defined the edges in the elastic network using a distance cutoff of 10 Å.

Comparison with AlphaFlow and ESMFlow. We compared our approach with the flow-matching based frameworks AlphaFlow and ESMFlow on a subset of 824 proteins out of a total of 1 117 comprised in the test set of PETIMOT-default. The 293 protein we excluded were too long (>450 amino acids) to be handled by AlphaFlow and ESMFlow in a reasonable amount of time using our computing resources. We downloaded the distilled "PDB" models from https://github.com/bjing2016/alphaflow. We executed AlphaFlow using the following command,

```
python predict.py --noisy_first --no_diffusion --mode alphafold
--input_csv seqs.csv --msa_dir msa_dir/
--weights alphaflow_pdb_distilled_202402.pt --samples 50
--outpdb output pdb/
```

AlphaFlow relies on OpenFold (Ahdritz et al., 2024) to retrieve the input multiple sequence alignment (MSA). ESMFlow was launched using the same command with an additional --mode esmfold flag and its corresponding weights. We used AlphaFlow and ESMFlow to generate 50 conformations for each test protein and then we treated each ensemble as a conformational collection. We then

aligned all members of the created collections to the reference conformations of the ground-truth collections. We used the identity coverage weights here. Finally, from the aligned collections, we extracted the principal linear motions. We shall additionally mention that we did not filter or adapt our test set to the AlphaFlow and ESMFlow methods. In other words, there can be certain data leakage between AlphaFlow/ESMFlow train data and our test examples.

B.5 ABLATION STUDIES

1031 1032

1033

1034

1035 1036

1037

1039

1040

1041

1043

1046

1047 1048

1049 1050

1051

1052

1055 1056

1057

1058

1061

1062

1064

1067

1068 1069

1070

1071

1074

1075

1077

1078

To understand the impact of different components on the performance of our model, we carried out ablation studies. We list them blow.

Model architecture variations.

- Network depth: We experimented with different numbers of message-passing layers (5 and 10 layers compared to our default value of 15 layers).
- Layer sharing: We tested a variant where all message-passing layers share the same parameters, as opposed to our default where each layer has unique parameters.
- Reduced internal embedding dimension: We tested a model with a smaller internal embedding dimension of 128 instead of the default 256.

Figure B.1 shows the evaluation of these modifications. A shallow 5-layers network underperforms on all evaluation metrics. The difference between other variants is not very significant.

Structure and sequence information ablation.

- Structure ablation: We removed all structural information from the model to assess the
 importance of geometric features and the performance with the PLM embeddings only. We
 did it by removing the edge attributes of the input of the message passing MLP.
- Sequence ablation: We ablated sequence information by replacing protein language model embeddings with random embeddings, testing them both with and without structural information.
- Embedding variants: We evaluated a different protein language model (ESMC-600M), both with and without structural tokens.

The evaluation results are shown in Fig. B.2. The results demonstrate that while both ProstT5 and ESM-Cambrian 600M perform similarly when combined with structural information, removing structural features leads to markedly different outcomes. ProstT5 embeddings partially compensate for the missing structural information, likely due to their structure-aware training, while relying solely on ESM-C embeddings results in poor performance.

Problem formulation ablation. We analyzed different combinations of our loss terms (compared to our default balanced weights of LS + SS):

- Least Square loss (LS): Using only the LS loss (weight 1.0).
- Squared Sinus loss (SS): Using only the SS loss (weight 1.0).
- Independent Subspaces (IS): Using only the IS loss (weight 1.0).

Figure B.3 compares three individual losses with the default option. The IS problem formulation underperforms on all the metrics. The default LS + SS formulation performs slightly better than those with individual loss components.

Graph connectivity ablation. We investigated different approaches to constructing the protein graph:

 Nearest neighbor-only: Using 15 nearest neighbors (sorted according to the corresponding Cα-Cα distances) without random edges.

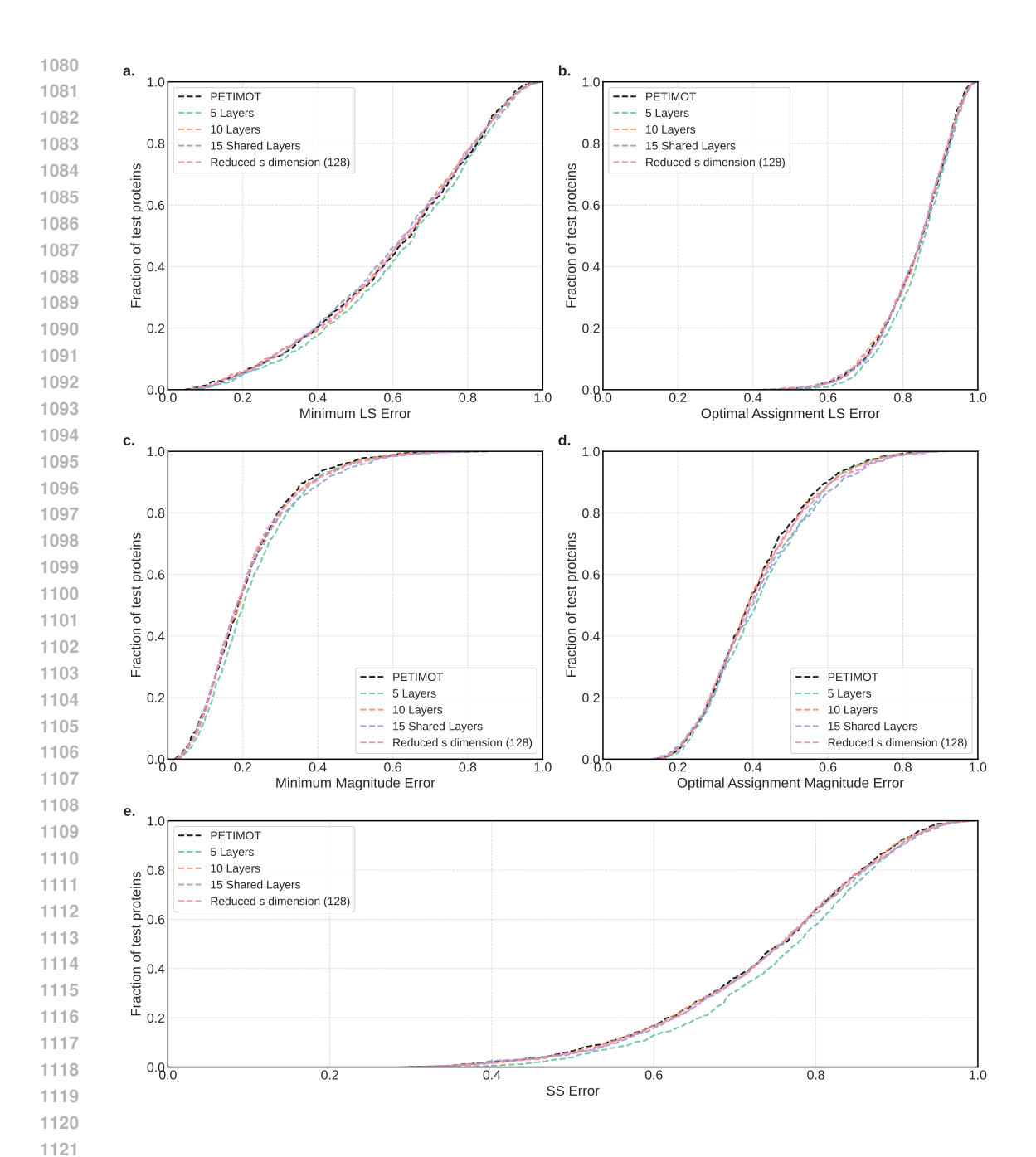


Figure B.1: **Network depth ablation.** We report cumulative curves for LS error (a-b), magnitude error (c-d), and SS error (e). For each protein, we computed the error either for the best-matching pair of predicted and ground-truth vectors (a,c) or for the best combination of four pairs of predicted and ground-truth vectors (b,d). We vary the number of layers in the network and the embedding dimension.

- Random connections-only: Using 15 random edges without nearest neighbors. This set is updated between every layer at each epoch.
- Static connectivity: Using a fixed set of random neighbors between the layers. This set is updated at each epoch.

Figure B.4 shows the ablation results. We can see that the nearest neighbor-only setup underperforms on all the metrics. Among other options, the random connectivity-only option gets lower results

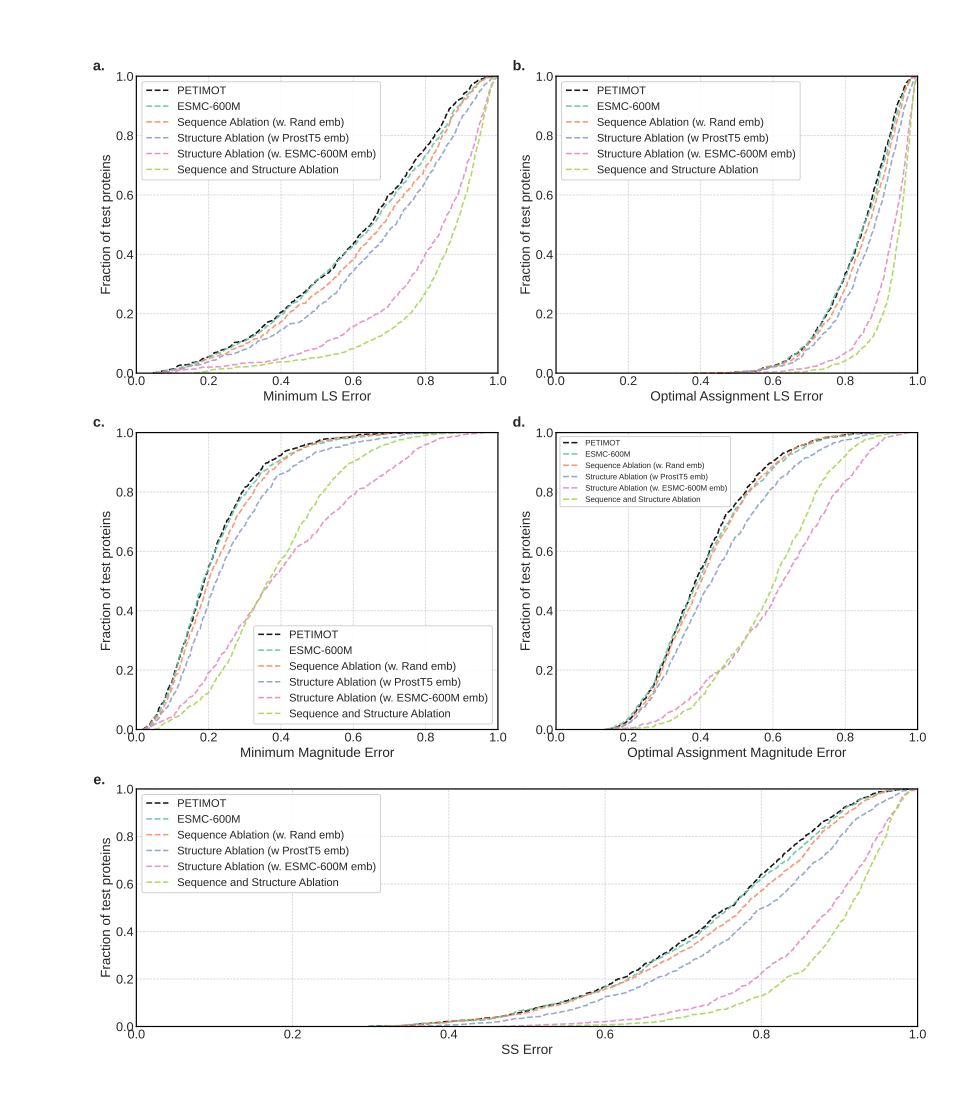


Figure B.2: Structure and sequence information ablation study. We report cumulative curves for LS error (a-b), magnitude error (c-d), and SS error (e). For each protein, we computed the LS and magnitude errors either for the best-matching pair of predicted and ground-truth vectors (a,c) or for the best combination of four pairs of predicted and ground-truth vectors (b,d).

at higher metrics values. The default option performs on par with the static connectivity, showing slightly better results on the optimal assignment magnitude error metrics.

B.6 ADDITIONAL VALIDATION ON ATLAS MOLECULAR DYNAMICS DATA

To further assess our model's generalization capabilities, we conducted an additional validation experiment using molecular dynamics (MD) data from the ATLAS database. This experiment provided an independent test of PETIMOT's performance on high-quality data with distinct characteristics from our training data.

The ATLAS MD dataset underwent a systematic preprocessing pipeline. First, we extracted the principal components from the MD trajectories. Subsequently, we assigned samples to appropriate cross-validation folds, ensuring strict exclusion of both structural and sequential similarity between training and test sets. This rigorous assignment process yielded 400 samples suitable for evaluation. The inference was then performed by applying our trained PETIMOT models to predict the conformational motions for each sample.

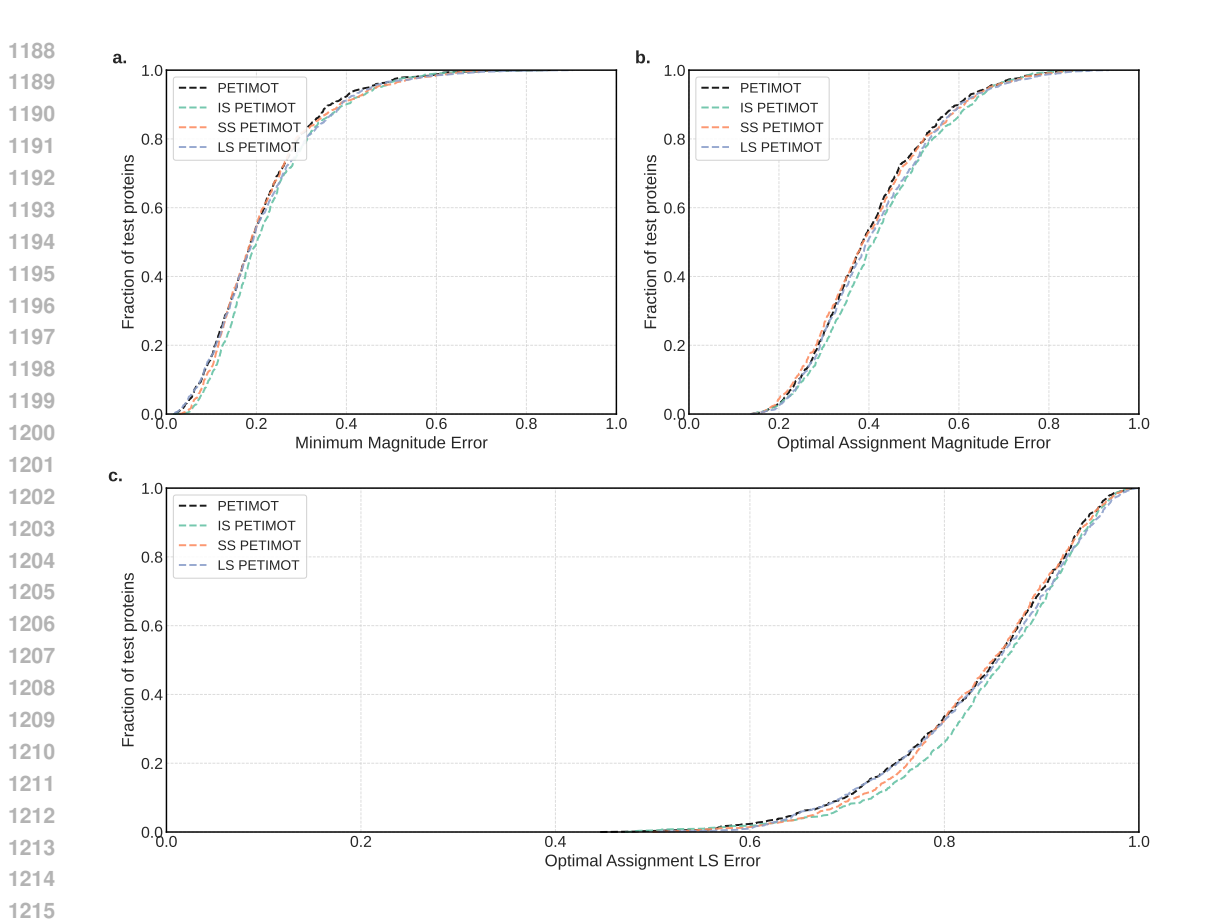


Figure B.3: **Performance comparison of different problem formulations.** We report cumulative curves for magnitude error (a,b) and LS error (c). For each protein, we computed the error either for the best-matching pair of predicted and ground-truth vectors (a) or for the best combination of four pairs of predicted and ground-truth vectors (b,c).

C ADDITIONAL RESULTS

Figure C.1 evaluates PETIMOT against NMA, ESMFlow and AlphaFlow approaches using additional metrics. These include the minimum magnitude error, the optimal assignment magnitude error, and the optimal assignment LS error. On all the metrics we see that PETIMOT outperforms the three other tested approaches.

We also experimented with a different number of predicted components, while maintaining the number of ground-truth components fixed at L=4. For these experiments, we trained additional models with the LS loss only:

- Single component prediction (1 mode).
- Reduced component prediction (2 modes).
- Extended component prediction (8 modes).

We compare these with our default setting of K=4 predicted components. Figure C.2 shows the results. The key insight is that minimum-based metrics (Fig. C.2a,c) and assignment-based metrics (Fig. C.2b,d) measure different aspects of subspace quality: Minimum metrics measure the best possible match between any predicted and ground-truth component. These improve with more predicted components (from 1 to 8) because having more candidates increases the likelihood of finding at least one good match with each ground-truth component. Optimal assignment metrics measure overall subspace alignment by finding the best one-to-one matching between predicted and ground-truth components. Here, models with fewer predicted components (1-2) perform better

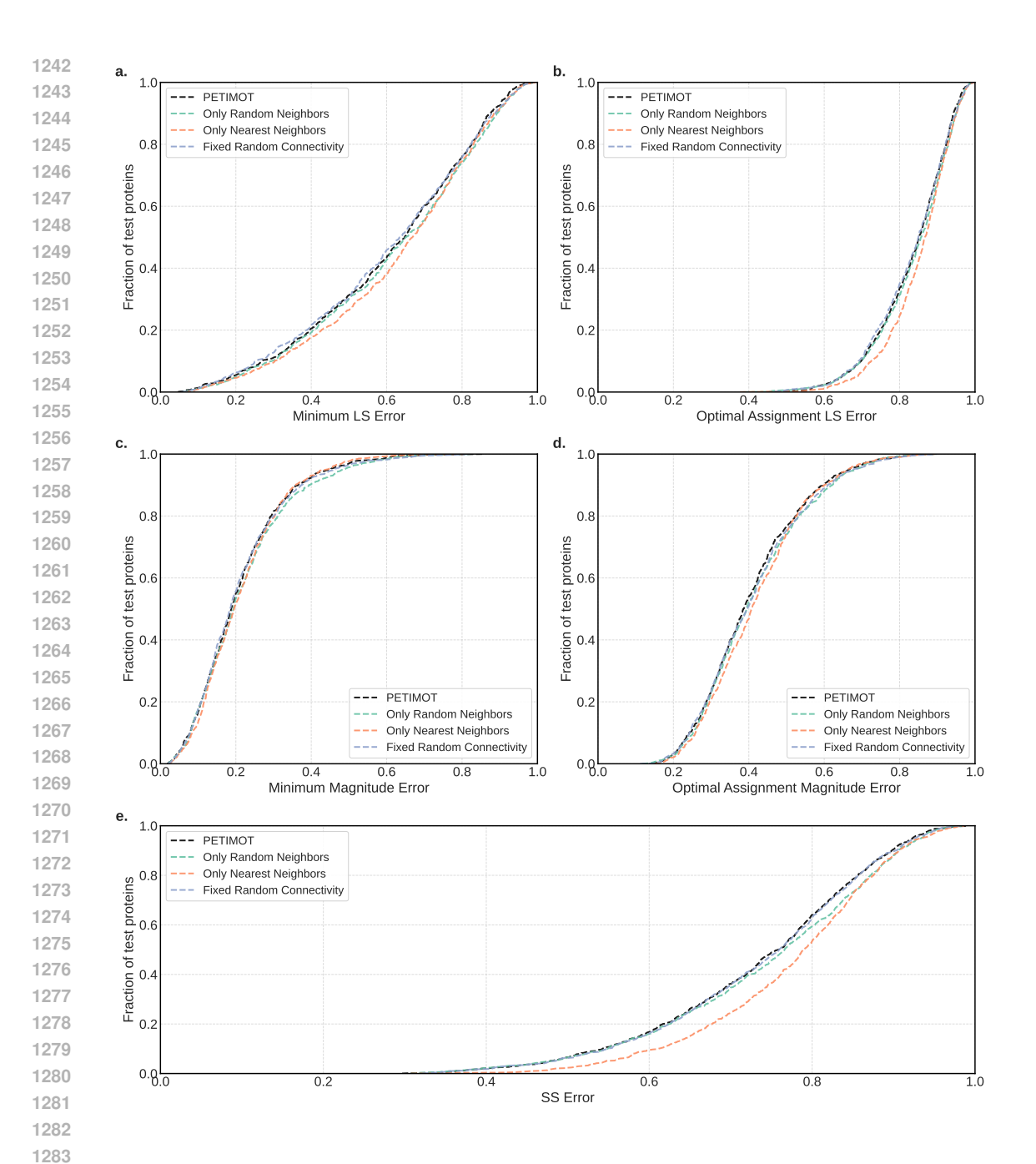


Figure B.4: **Graph connectivity ablation.** We report cumulative curves for LS error (a-b), magnitude error (c-d), and SS error (e). For each protein, we computed the error either for the best-matching pair of predicted and ground-truth vectors (a,c) or for the best combination of four pairs of predicted and ground-truth vectors (b,d). Only Random Neighbors: each residue (node) is connected to 15 randomly chosen residues and the connectivity changes after each layer. Only Nearest Neighbors: each residue (node) is connected to its 15 nearest neighbors in the input 3D structure. Fixed Random Connectivity: each residue (node) is connected to 15 residues randomly chosen at the beginning.

because they face fewer constraints in the assignment problem - each predicted component can be matched to the best available ground-truth component without competition. The 8-component model maintains the best performance overall, as having more candidate vectors provides flexibility while still capturing the 4-dimensional ground-truth subspace effectively.

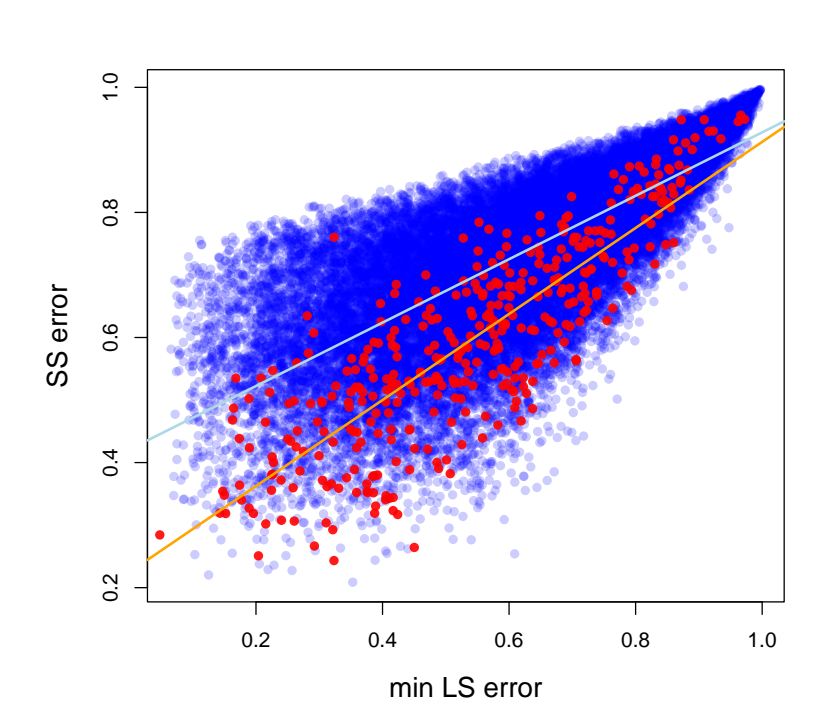


Figure B.5: **SS error in function of min LS error.** Blue dots are samples from our PDB dataset while red dots correspond to the ATLAS MD samples.

Figure C.3 compares the accuracy of the predicted test proteins (minimum LS loss) with the structural (TM-score) and sequence (sequence identity) distances to the training set. We do not see a clear correlation between the prediction accuracy and the similarity to the training examples. Please also see Fig. 2b-c for comparison.

Figure C.4 further assesses PETIMOT's generalisation capability across protein families. To do so, we implemented a more stringent train-validation-test split using a 30% sequence similarity threshold (see main text and Appendix B.4). When trained under this stringent protocol, PETIMOT still substantially outperforms all baseline methods according to minimum L and SS metrics (Fig. C.4a-b). Moreover, we observe a slight generalisation improvement of *PETIMOT-stringent* over *PETIMOT-default* on a test set of 474 proteins evolutionary distant from any protein used for training or validation of any of the two model versions (Fig. C.4c-d).

Figures C.5 and C.6 show predicted (blue arrows) and ground-truth (red arrows) motion vectors for the xylanase A from *Bacillus subtilis* and the periplasmic domain of Gliding motility protein GldM from *Capnocytophaga canimorsus*, respectively.

D LICENSES FOR USED RESOURCES

In this work, we utilize several existing resources. The protein structures were obtained from the Protein Data Bank (PDB, https://www.rcsb.org/, version accessed on June 2023) which is distributed under the CC0 1.0 Universal Public Domain Dedication license (CC0 1.0). We complemented PDB data with data from PDB-redo (accessed June 2023) developed by Joosten *et al.* (Joosten et al., 2014), available at https://pdb-redo.eu under the licence specified at https://pdb-redo.eu/license. For protein language modeling, we employed ProstT5 developed by Heinzinger *et al.* (Heinzinger et al., 2023), available under the MIT license at https://huggingface.co/Rostlab/ProstT5, and ESM-Cambrian 600M (verison esmc-600m-2024-12) developed by the EvolutionaryScale Team (ESM Team, 2024), available under the

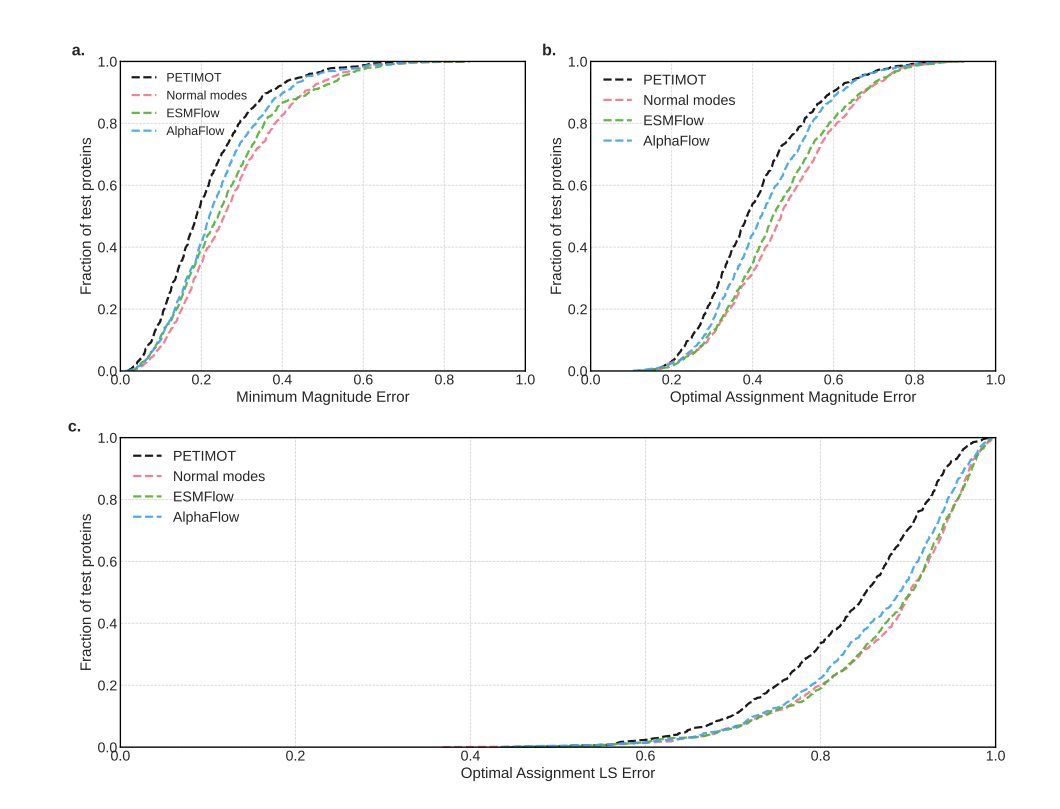


Figure C.1: **Performance comparison with other methods on the test proteins.** We report cumulative curves for magnitude error (a,b) and LS error (c). For each protein, we computed the error either for the best-matching pair of predicted and ground-truth vectors (a) or for the best combination of four pairs of predicted and ground-truth vectors (b,c).

Cambrian Non-Commercial License at https://huggingface.co/EvolutionaryScale/esmc-600m-2024-12. Additional resources include the DANCE method (version of Oct 8, 2024) developed by Lombard et al., available under the MIT license at https://github.com/PhyloSofS-Team/DANCE. As baselines, we ran the NOLB method (version 1.9) developed by Hoffmann et al. (Hoffmann & Grudinin, 2017) and available at https://team.inria.fr/nano-d/software/nolb-normal-modes/, and the AlphaFlow (version AlphaFlow-PDB distilled) and ESMFlow (version ESMFlow-PDB distilled) models developed by Jing et al. (Jing et al., 2024) and available at https://github.com/bjing2016/alphaflow. We used TM-align (version 20220412) developed by Zhang and Skolnick (Zhang & Skolnick, 2005) and available at https://zhanggroup.org/TM-align/to perform all-to-all pairwise structural alignments between train and test protein conformations and compute TM-scores.

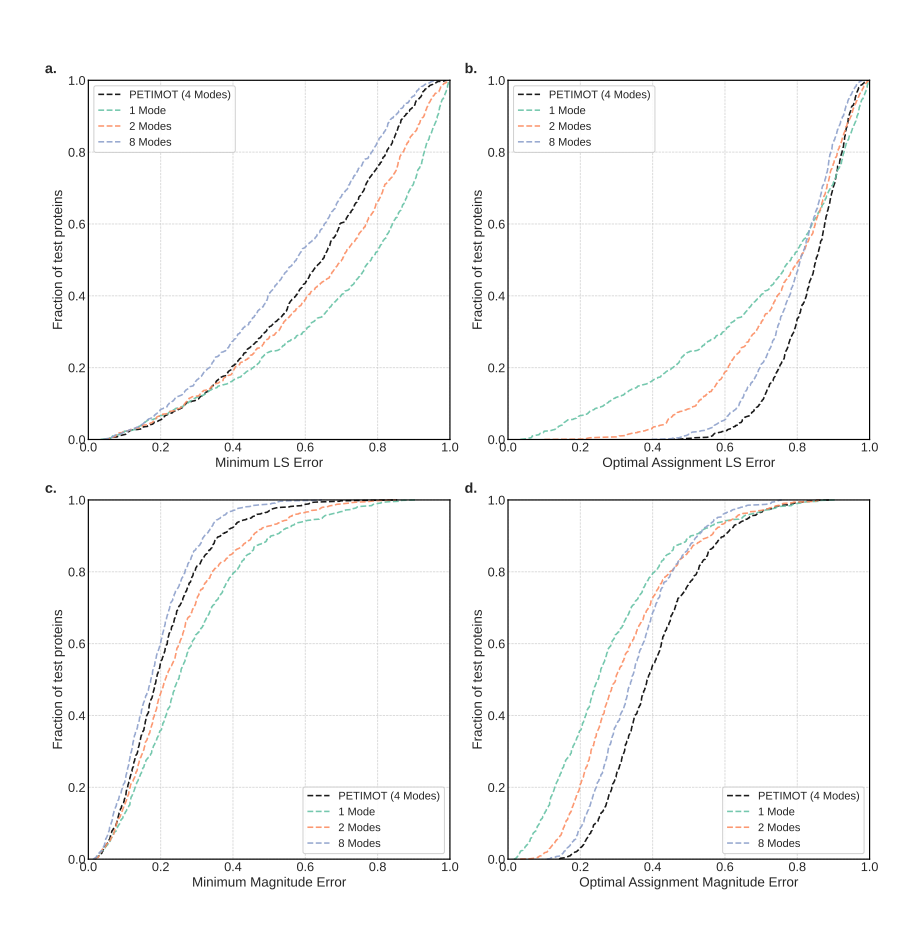


Figure C.2: **Impact of the number of predicted components.** We report cumulative curves for LS error (a-b) and magnitude error (c-d). For each protein, we computed the error either for the best-matching pair of predicted and ground-truth vectors (a,c) or for the best combination of all pairs of predicted and ground-truth vectors using optimal linear assignment (b,d). We compare models trained to predict different numbers of components (modes): 1, 2, 4, or 8, using only the LS loss.

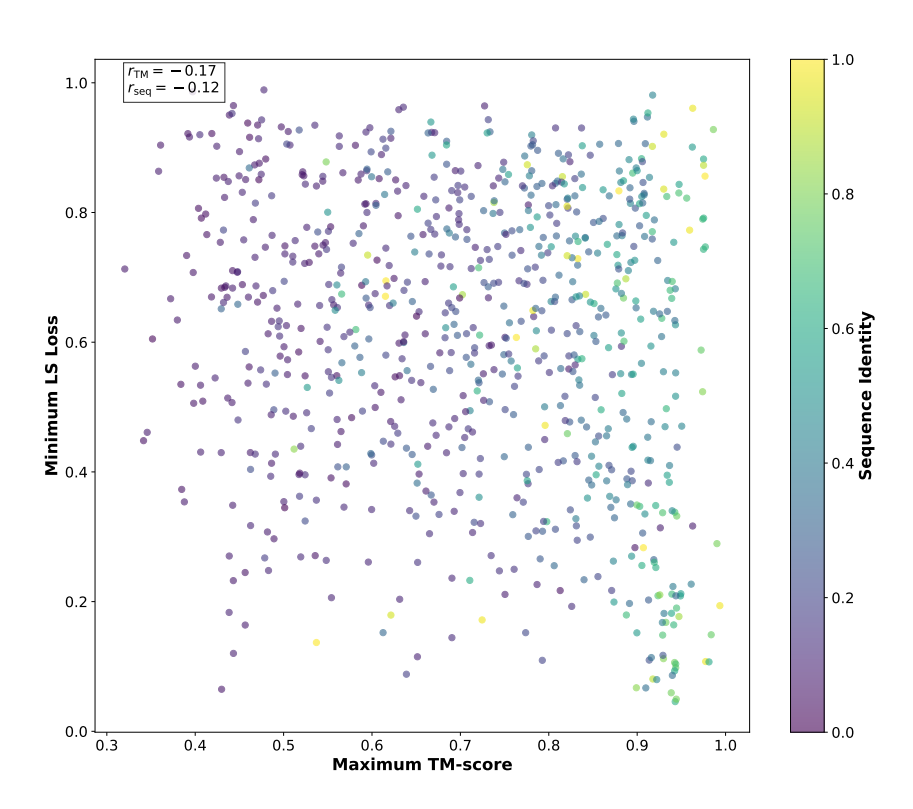


Figure C.3: Relationship between PETIMOT's prediction accuracy and structural/sequence similarity with the training set. The minimum LS error is plotted against the maximum TM-score between each test protein and any protein in the training set. Points are colored by the maximum sequence identity to the training samples.

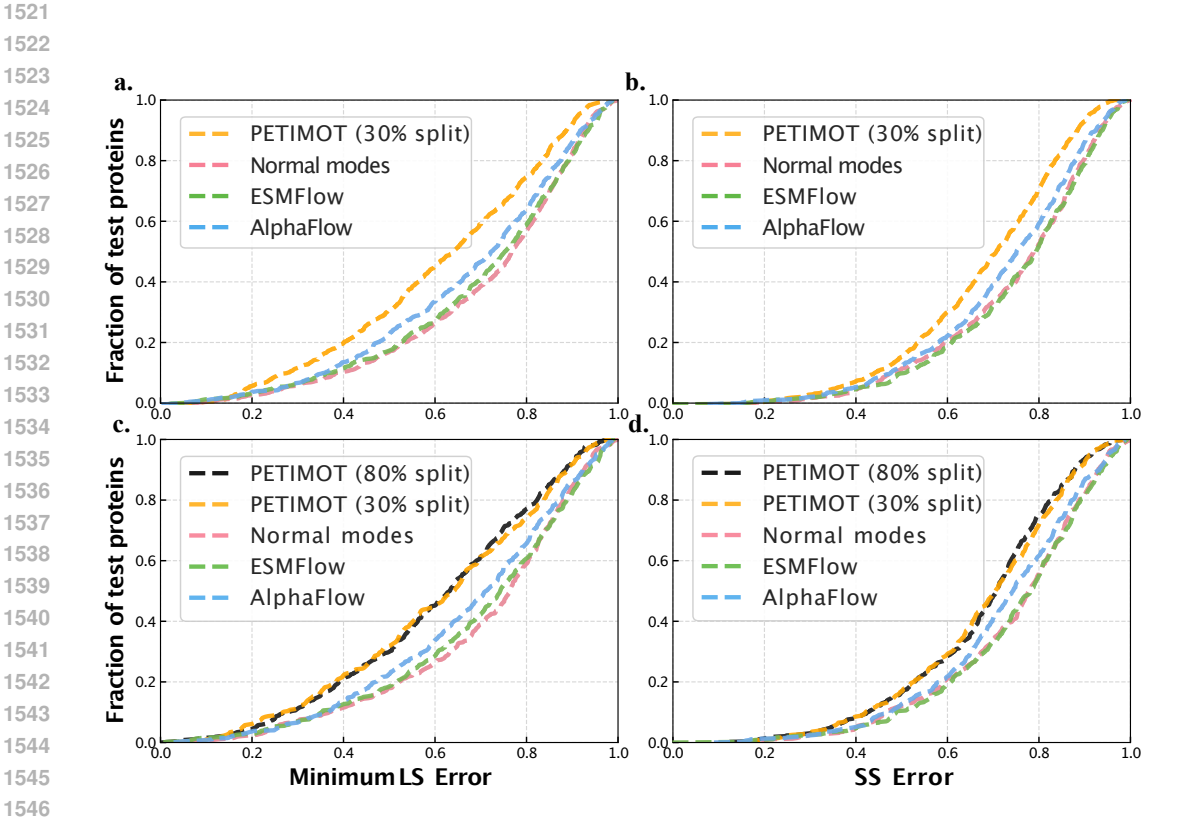


Figure C.4: Cumulative error curves computed on the test proteins. a-b. Comparison between PETIMOT-stringent model and three other methods on a non-redundant set of 734 test proteins. PETIMOT-stringent was trained on a stringent and non-redundant training-validation-test split defined using a 30% sequence identity threshold. c-d. Comparison between PETIMOT-default, PETIMOTstringent and three other methods on 474 test proteins that share less than 30% sequence similarity with any protein used in training or validation of either model. a,c. Minimum LS error corresponding to the best matching pair of predicted and ground-truth motions. b,d. SS error computed between the entire predicted and ground-truth subspaces.

Figure C.5: Visualization of predicted (blue arrows) and ground-truth (red arrows) motion vectors for PDB structure 3EXU (chain A), with LS error of 0.20. The predicted deformation was used to generate the interpolated conformations shown in Fig. 2b.

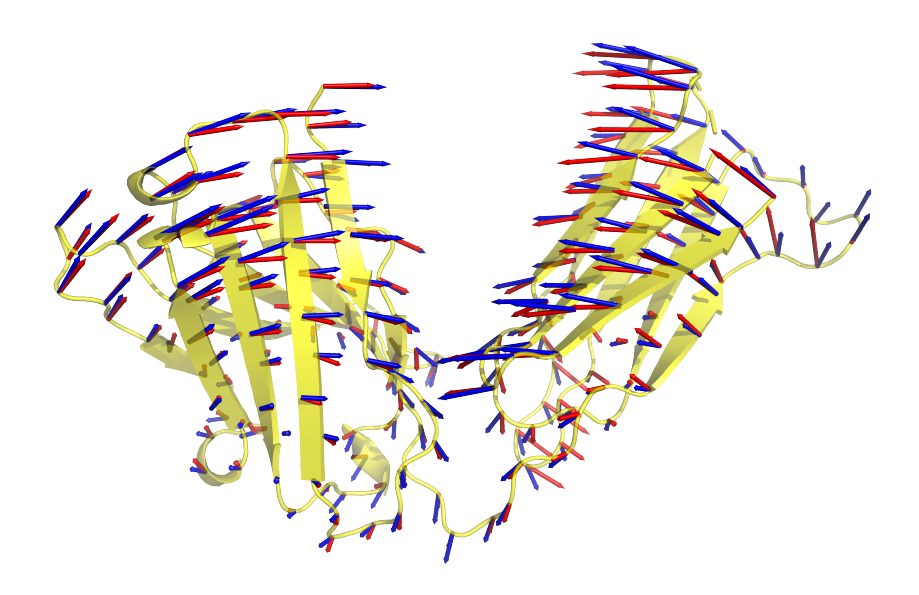


Figure C.6: Visualization of predicted (blue arrows) and ground-truth (red arrows) motion vectors for PDB structure 7SD2, with LS error of 0.18. The predicted deformation was used to generate the interpolated conformations shown in Fig. 2c.